Journal of Medicinal Chemistry Article

J. Med. Chem. **2009,** *52,* 5365–5379 **5365**
DOI: 10.1021/jm900859q

Pyrano[3,2-*c*]quinoline−6-Chlorotacrine Hybrids as a Novel Family of Acetylcholinesterase- and β-Amyloid-Directed Anti-Alzheimer Compounds

Pelayo Camps,[†] Xavier Formosa,[†] Carles Galdeano,[†] Diego Muñoz-Torrero,*[,†] Lorena Ramírez,[†] Elena Gómez,[‡] Nicolás Isambert,[‡] Rodolfo Lavilla,[‡,⊥] Albert Badia,[§] M. Victòria Clos,[§] Manuela Bartolini,[#] Francesca Mancini,[#] Vincenza Andrisano,[#] Mariana P. Arce,[∞] M. Isabel Rodríguez-Franco,[∞] Óscar Huertas,[∥] Thomai Dafni,[∥] and F. Javier Luque[∥]

[†]*Laboratori de Química Farmacèutica* (*Unitat Associada al CSIC*), *Facultat de Farmàcia, and Institut de Biomedicina* (*IBUB*), *Universitat de Barcelona, Av. Diagonal 643, E-08028, Barcelona, Spain,* [‡]*Institute for Research in Biomedicine, Barcelona Science Park, Baldiri Reixac 10-12, E-08028, Barcelona, Spain,* [⊥]*Laboratori de Química Orgànica, Facultat de Farmàcia, Universitat de Barcelona, Av. Joan XXIII, s/n, E-08028, Barcelona, Spain,* [§]*Departament de Farmacologia, Terapèutica i Toxicologia, Institut de Neurociències, Universitat Autònoma de Barcelona, E-08193, Bellaterra, Barcelona, Spain,* [#]*Department of Pharmaceutical Sciences, Alma Mater Studiorum, Bologna University, Via Belmeloro 6, I-40126, Bologna, Italy,* [∞]*Instituto de Química Médica* (*CSIC*), *Juan de la Cierva, 3, E-28006, Madrid, Spain, and* [∥]*Departament de Fisicoquímica, Facultat de Farmàcia, and Institut de Biomedicina* (*IBUB*), *Universitat de Barcelona, Av. Diagonal 643, E-08028, Barcelona, Spain*

Received March 16, 2009

Two isomeric series of dual binding site acetylcholinesterase (AChE) inhibitors have been designed, synthesized, and tested for their ability to inhibit AChE, butyrylcholinesterase, AChE-induced and self-induced β-amyloid (Aβ) aggregation, and β-secretase (BACE-1) and to cross blood−brain barrier. The new hybrids consist of a unit of 6-chlorotacrine and a multicomponent reaction-derived pyrano[3,2-*c*]-quinoline scaffold as the active-site and peripheral-site interacting moieties, respectively, connected through an oligomethylene linker containing an amido group at variable position. Indeed, molecular modeling and kinetic studies have confirmed the dual site binding of these compounds. The new hybrids, and particularly **27**, retain the potent and selective human AChE inhibitory activity of the parent 6-chlorotacrine while exhibiting a significant in vitro inhibitory activity toward the AChE-induced and self-induced Aβ aggregation and toward BACE-1, as well as ability to enter the central nervous system, which makes them promising anti-Alzheimer lead compounds.

Introduction

In the past decade, the design of novel classes of inhibitors of the enzyme acetylcholinesterase (AChE[a]) as therapeutic interventions for Alzheimer's disease (AD) has been mostly driven by the pivotal finding that AChE can bind the β-amyloid peptide (Aβ), thereby promoting Aβ aggregation as an early event in the neurodegenerative cascade of AD.[1,2] The Aβ proaggregating effect of AChE results in cognitive impairment in doubly transgenic mice expressing human amyloid precursor protein (APP) and human AChE.[3,4] Blockade of the peripheral site of AChE, the Aβ recognition zone within the enzyme,[5] was therefore expected to affect the AChE-induced Aβ aggregation and could be a potential strategy to modulate the progression of AD.

On the basis of these premises, novel classes of AChE inhibitors (AChEIs) targeting the peripheral site have emerged as promising disease-modifying anti-Alzheimer drug candidates.[6] Of particular interest are those AChEIs able to simultaneously bind to both peripheral and catalytic sites, which are separated by about 14 Å, as they are located at the mouth and at the bottom of the gorge leading to the active site.[7] Apart from the Aβ antiaggregating effects arising from blockade of the peripheral site, dual binding site AChEIs are usually endowed with a potent AChE inhibitory activity because of the increased number of drug−target interactions, thus overcoming the low activity of selective peripheral site AChEIs.[8−18] Indeed, in vitro inhibitory activities of AChE and AChE-induced Aβ aggregation have been reported for different families of dual binding site AChEIs,[19−34] which in cases such as memoquin[26,27] and NP-61[35] have been shown to reduce brain amyloid burden and increase cognition in animal models of AD. Some dual binding site AChEIs such as memoquin[26,27] or bis(7)-tacrine[9,13,36,37] are undergoing preclinical evaluation, while NP-61 entered phase I clinical trials for AD in the U.K. in April 2007.[38] Prompted by these results and the tremendous potential of dual binding site AChEIs to impact both the course of AD and its symptomatology, the design and synthesis of novel families of dual binding site AChEIs have been actively pursued in the past years.[39−52]

The design of dual binding site AChEIs is carried out by linking through a tether of suitable length an active-site interacting unit, usually derived from a known active site AChEI, with a peripheral-site interacting unit suited to interact with Trp286 (human AChE (hAChE) numbering), the

*To whom correspondence should be addressed. Phone: +34 + 934024533. Fax: +34 + 934035941. E-mail: dmunoztorrero@ub.edu.

[a] Abbreviations: Aβ, β-amyloid peptide; AChE, acetylcholinesterase; AChEI, acetylcholinesterase inhibitor; AD, Alzheimer's disease; APP, amyloid precursor protein; bAChE, bovine acetylcholinesterase; BACE-1, β-secretase; BBB, blood−brain barrier; BChE, butyrylcholinesterase; CNS, central nervous system; DDQ, 2,3-dichloro-5,6-dicyano-1,4-benzoquinone; DTNB, 5,5′-dithiobis(2-nitrobenzoic) acid; hAChE, human acetylcholinesterase; hBChE, human butyrylcholinesterase; HFIP, 1,1,1,3,3,3-hexafluoro-2-propanol; PAMPA, parallel artificial membrane permeation assay; PBS, phosphate buffered saline; PDB, Protein Data Bank; PTFE, polytetrafluoroethylene; *Tc*AChE, *Torpedo californica* acetylcholinesterase.

Published on Web 08/07/2009

characteristic residue of the peripheral site. With a few exceptions in which a peripheral-site interacting unit containing an aliphatic amine, protonated at physiological pH, or a quaternary ammonium group establishes cation−π interactions with Trp286, in most cases the peripheral-site interacting unit contains aromatic moieties able to establish $\pi-\pi$ stacking interactions with Trp286, in some cases reinforced by concomitant cation−π interactions due to the presence of protonatable or quaternary nitrogen atoms in the aromatic system. The prototype of peripheral site AChEI is propidium (**1**, Chart 1), which binds the AChE peripheral site in two orientations related by a flip of 180° around the phenanthridinium pseudosymmetry axis.[53,54] The driving force for the binding of **1** to the peripheral site is the $\pi-\pi$ stacking, reinforced by cation−π interactions, between the phenanthridinium moiety and Trp286, which is supplemented by a hydrogen bond between one of the aromatic amino groups and His287.

Some of us recently reported the synthesis of the multicomponent reaction-derived pyrano[3,2-*c*]quinoline scaffold **2** (Chart 1).[55] We thought that a 5-phenyl-substituted derivative thereof would resemble the 6-phenylphenanthridinium moiety of propidium and could serve as the peripheral-site interacting unit of a novel family of dual binding site AChEIs. Because the nitrogen atom of this tricyclic moiety is not expected to be protonated at physiological pH (Table S1, Supporting Information), this aromatic system should establish $\pi-\pi$ stacking with Trp286. Noteworthy, the neutral character of this moiety could result in a better penetration into the central nervous system (CNS).

Herein, we describe the synthesis, pharmacological evaluation, and molecular modeling of a novel family of potent dual binding site AChEIs that combine a 5-phenylpyrano[3,2-*c*]quinoline moiety with 6-chlorotacrine, **3** (Chart 1), a potent AChEI already used in other dual binding site AChEIs,[22,23,31,32,39,44,52,56,57] through an amido-containing oligomethylene linker. The pharmacological evaluation of these novel compounds includes AChE and butyrylcholinesterase (BChE) inhibition, as well as inhibition of the AChE- and self-induced Aβ aggregation and inhibition of β-secretase (BACE-1), which altogether comprises an interesting set of effects shared by some dual binding site AChEIs. To prove the starting hypothesis on a good blood−brain barrier (BBB) permeability, the brain penetration of the novel hybrids has been assessed using an artificial membrane assay.

Chemistry

The structures of the novel 5-phenylpyrano[3,2-*c*]-quinoline−6-chlorotacrine hybrids **18**−**27** are shown in Scheme 2. Alignment of the 5-phenylpyrano[3,2-*c*]quinoline system with the phenanthridinium moiety of propidium in its complex with mouse AChE[53] (Figure S1, Supporting Information) revealed that if the novel hybrids were to interact with AChE by placing the tricyclic system in a way similar to that of the tricyclic system of propidium, position 9 of the pyrano[3,2-*c*]quinoline system would be suitable for attachment of the linker, which from this point could snake down the active site gorge. An ester group at position 9 was chosen as a suitable functionalization to allow attachment of the linker by reaction with an appropriate aminoalkyltacrine. Thus, tricyclic ester **11** (Scheme 1) was designed as the precursor of the peripheral-site interacting unit of the novel hybrids **18**−**22** (Scheme 2).

Chart 1. Structures of Propidium, Scaffold **2**, and 6-Chlorotacrine

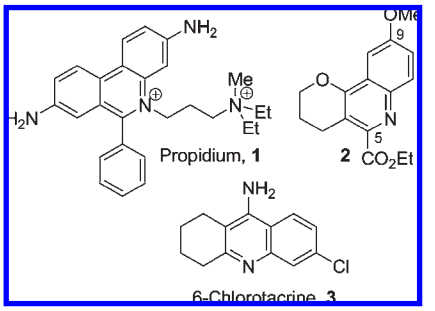

Scheme 1. Synthesis of Tricyclic Esters **11** and **12** and Carboxylic Acids **13** and **14**

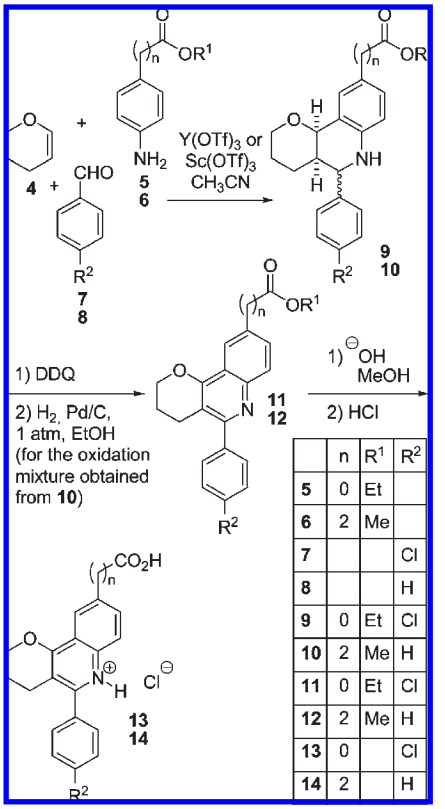

	n	R^1	R^2
5	0	Et	
6	2	Me	
7			Cl
8			H
9	0	Et	Cl
10	2	Me	H
11	0	Et	Cl
12	2	Me	H
13	0		Cl
14	2		H

Recently, Martínez and co-workers developed a novel series of indole−tacrine hybrids as dual binding site AChEIs, which contained an amido group within the linker either directly bound to the indole system (i.e., the peripheral-site interacting unit) or separated by one to three atoms (methylene groups in most cases), and reported important differences in the AChE inhibitory activity upon shift of the amido group within the tether chain while keeping the same total length of the linker.[23] Specifically, separation of the amide from the indole ring by two methylene groups increased up to 2300-fold the AChE inhibitory potency relative to the indole directly bound counterpart. In view of these results, we designed the tricyclic ester **12** (Scheme 1) as the precursor of the parallel series of hybrids **23**−**27** (Scheme 2), containing linkers of the same total length as **18**−**22** but with the amido group shifted two positions within the tether. Regarding the length of the linker, oligomethylene chains of 6−10 and 4−8 members for hybrids **18**−**22** and **23**−**27**, respectively, were considered suitable to provide the dual site binding.

Scheme 2. Synthesis of Hybrids **18**−**27**

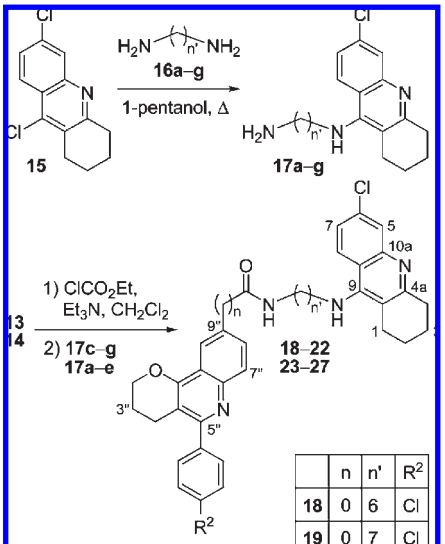

16, 17	n'
a	4
b	5
c	6
d	7
e	8
f	9
g	10

	n	n'	R^2
18	0	6	Cl
19	0	7	Cl
20	0	8	Cl
21	0	9	Cl
22	0	10	Cl
23	2	4	H
24	2	5	H
25	2	6	H
26	2	7	H
27	2	8	H

The synthesis of hybrids **18**−**27** was envisaged through the coupling of tricyclic esters **11** and **12** with readily available aminoalkyltacrines **17**.[23] A straightforward access to **11** and **12** was carried out through a Povarov multicomponent reaction.[58] Thus, reaction of 3,4-dihydro-2*H*-pyran, **4**, with ethyl *p*-aminobenzoate, **5**, and *p*-chlorobenzaldehyde, **7**, under $Y(OTf)_3$ catalysis in CH_3CN afforded in 76% yield a 1.3:1 diastereomeric mixture of pyranotetrahydroquinolines **9**, whose 2,3-dichloro-5,6-dicyano-1,4-benzoquinone (DDQ) oxidation[55] yielded the desired tricyclic ester **11** in 75% yield. The Povarov reaction of methyl 3-(4-aminophenyl)propanoate **6**[59] with **4** and benzaldehyde **8** under $Sc(OTf)_3$ catalysis, followed by DDQ oxidation of the diastereomeric mixture of pyranotetrahydroquinolines **10** and catalytic hydrogenation of the unseparable mixture of the desired ester **12** and its cinnamate derivative, formed by the competitive oxidation of the ethylene bridge, afforded in 82% overall yield the tricyclic ester **12** (Scheme 1). This latter compound lacked the chlorine atom at the phenyl substituent, present in **11**. However, this chlorine atom, easily removable in the catalytic hydrogenation conditions, was not expected to play a major role in the interaction of this moiety with the AChE peripheral site.

Aminoalkyltacrines **17a**−**g** were synthesized in 35−78% yield following a procedure[23,60,61] that involves amination of dichloroacridine **15**[62] with commercially available α,ω-diamines **16a**−**g** in refluxing 1-pentanol (Scheme 2). In this reaction, significant amounts of dimers of 6-chlorotacrine, **28a**−**g**,[56,62,63] were formed despite the fact that an excess of diamines (4 equiv) was used.

Hydrolysis of esters **11** and **12** (Scheme 1), followed by treatment of the corresponding carboxylic acids **13** and **14** with 1 equiv of ethyl chloroformate and 2.2 equiv of Et_3N in CH_2Cl_2, and reaction of the resulting mixed anhydrides with 1 equiv of aminoalkyltacrines **17c**−**g** and **17a**−**e**, respectively, afforded hybrids **18**−**22** and **23**−**27** in low to moderate yields (19−37% and 25−48% yield, respectively). The novel hybrids **18**−**27** were fully characterized as dihydrochlorides through their spectroscopic data, HRMS, and elemental analyses. Not unexpectedly, in a study to assess the potential chemical instability at physiological pH of the new hybrids due to the presence of a hydrolyzable amido group, hybrid **23** did not undergo any noticeable decomposition in 1:1 acetonitrile/Sorensen phosphate buffer at pH 7.4 up to 4 days at 37 °C (see Supporting Information).

Pharmacology and Molecular Modeling

Cholinesterase Inhibition. AChE Inhibition. The AChE inhibitory activity of hybrids **18**−**27** was assayed by the method of Ellman et al.[64] on AChE from bovine (bAChE) and human (hAChE) erythrocytes (Table 1). The hybrids of the first series (**18**−**22**) are potent inhibitors of both bAChE and hAChE, with IC_{50} values in the low nanomolar range in most cases. The most potent hAChE inhibitor was **20**, and shortening or lengthening of the linker led to a 3- to 7-fold decrease of inhibitory activity. The hybrids of the second series (**23**−**27**) are also potent inhibitors of both enzymes. In contrast with the first series, hybrids **23**−**27** turned out to be 2- to 3-fold more potent toward the human enzyme. Also, unlike the first series, no significant dependency on the length of the linker was found for the hAChE inhibitory activity of **23**−**27**. Hybrids **24** and **25** were the most potent hAChE inhibitors of the second series, they being roughly equipotent to compound **20**, in which the total length of the linker is equivalent to that of **25**. Although dual site binding to AChE is expected to increase the inhibitory potency relative to the monomeric parent compounds from which they were designed, this assumption is not always fulfilled.[65,66] Indeed, the hAChE inhibitory activity of hybrids **20**, **24**, and **25** is comparable with that of the parent 6-chlorotacrine and is clearly higher than the activity measured for propidium and the tricyclic ester precursors **11** and **12**.

Molecular Modeling Studies. To gain insight into the molecular determinants that modulate the hAChE inhibitory activity of the novel hybrids, the binding mode of compounds **20**, **25**, and **27** was investigated by means of docking computations.

The conformation of the active site gorge appears to be highly conserved in different X-ray crystallographic structures. In particular, the observed structural changes at the catalytic binding site are small except for those of Tyr337 (in hAChE; Phe330 in *Torpedo californica* AChE, *Tc*AChE).[67,68] Accordingly, the binding mode of the 6-chlorotacrine unit of these hybrids can be inferred from the X-ray crystallographic structures of *Tc*AChE complexes with tacrine[7] and its structurally related analogue huprine X,[69] where the 9-aminotetrahydroacridine unit is stacked against Trp86 and Tyr337 (Trp84 and Phe330 in *Tc*AChE), the protonated pyridine nitrogen atom is hydrogen-bonded to His447 (His440 in *Tc*AChE), and the chlorine atom fits a hydrophobic pocket formed by Trp439, Met443, and Pro446 (Trp432, Met436, and Ile439 in *Tc*AChE). In fact, a common pose is found for the tacrine moiety in the X-ray structures of a variety of dual binding site inhibitors, including bis(5)-tacrine and bis(7)-tacrine,[70] tacrine(8)-4-aminoquinoline,[70] NF595,[71] tacrine(10)-hupyridone,[72] and TZ2PA6.[73] The structural features of the binding of the pyrano[3,2-*c*]-quinoline moiety of the hybrids at the peripheral site are

Table 1. AChE and BChE Inhibitory Activities of the Hydrochlorides of 6-Chlorotacrine and Tricyclic Esters **11** and **12**, Propidium Iodide, and the Dihydrochlorides of the Pyrano[3,2-*c*]quinoline−6-Chlorotacrine Hybrids[a]

	IC_{50} (nM)			
compd	bAChE	hAChE	hBChE	AChE selectivity[b]
18·2HCl	20.4 ± 0.9	19.2 ± 1.5	1074 ± 178	56
19·2HCl	10.3 ± 0.4	18.3 ± 2.6	1931 ± 47	106
20·2HCl	10.4 ± 0.7	7.03 ± 0.3	331 ± 42	47
21·2HCl	24.0 ± 1.6	24.9 ± 1.5	1391 ± 31	56
22·2HCl	93.7 ± 3.2	50.0 ± 3.0	1622 ± 117	32
23·2HCl	48.1 ± 2.0	16.6 ± 1.0	586 ± 16	35
24·2HCl	23.9 ± 1.3	9.64 ± 1.4	290 ± 9.8	30
25·2HCl	30.8 ± 1.9	11.1 ± 0.1	218 ± 3.2	20
26·2HCl	29.9 ± 0.6	14.4 ± 1.4	234 ± 7.8	16
27·2HCl	34.1 ± 1.0	14.0 ± 1.2	1076 ± 78	77
11·HCl	> 10000	> 10000	> 10000	nd[c]
12·HCl	> 10000	nd[c]	nd[c]	nd[c]
propidium iodide	6289 ± 377	32300 ± 2200[d]	13200 ± 400[d]	0.4
6-chlorotacrine·HCl	5.73 ± 0.4	8.32 ± 0.7	916 ± 19	110

[a] Values are expressed as the mean ± standard error of the mean of at least four experiments. IC_{50} inhibitory concentration (nM) of AChE (from bovine or human erythrocytes) or BChE (from human serum) activity. [b] IC_{50}(hBChE)/IC_{50}(hAChE). [c] Not determined. [d] Data from ref 21.

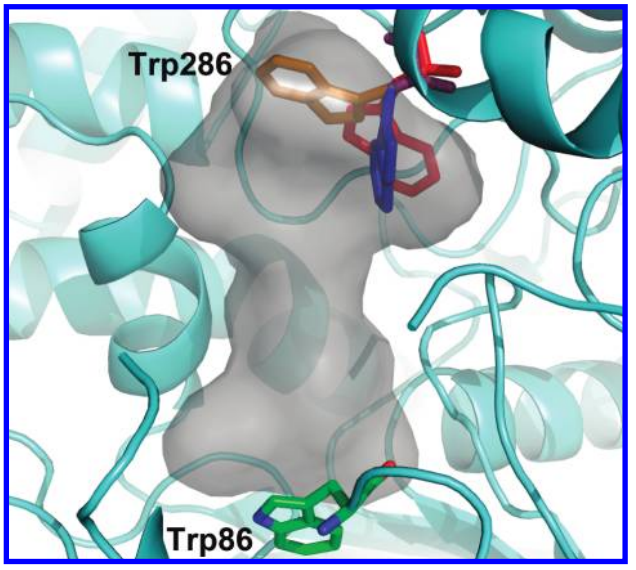

Figure 1. Representation of the three orientations adopted by Trp286 in targets A (blue), B (red), and C (orange) of hAChE (χ_1 and χ_2 amount to −60° and −80° for A, to −120° and +50° for B, and to −160° and −120° for C; see text). The backbone of hAChE is shown in ribbon (light-blue). Trp86 at the catalytic site is colored by atom, and the gorge leading from the peripheral site to the catalytic pocket is shown in gray.

more delicate because of the conformational flexibility of Trp286 (Trp279 in *Tc*AChE), as noted in the X-ray structures available for several peripheral site ligands,[53] including propidium, and dual binding site inhibitors[70−73] as well as from molecular dynamics simulations.[23,31,74] In fact, three main arrangements of the indole ring of Trp286 can be identified upon inspection of the X-ray structures (Table S2, Supporting Information). The first orientation is characterized by dihedral angles χ_1 (N−C_α−C_β−C_γ) and χ_2 (C_α−C_β−C_γ−$C_{\delta 2}$) close to −60°and −80°, respectively, as found in the apo form of the enzyme,[53,75] and in complexes with catalytic (tacrine,[7] huprine X,[69] and (−)-huperzine A[76]) and peripheral (propidium, decidium, and gallamine)[53] binding site inhibitors. Moreover, this arrangement is found in complexes with dual binding site inhibitors (decamethonium,[7] donepezil,[77] bis(5)-tacrine,[70] tacrine(10)-hupyridone,[72] and anti-TZ2PA6[73]) and in the complex with fasciculin.[78] Dihedral angles close to −120° (χ_1) and +50° (χ_2) are found in complexes with bis(7)-tacrine,[70] tacrine(8)-4-aminoquinoline,[70] and NF595.[71] At this point, it is worth stressing how the different lengths of the tether in bis(5)-tacrine and bis(7)-tacrine lead to a distinct arrangement of the indole ring of Trp286.[70] Finally, an alternative orientation defined by dihedral angles close to −160° (χ_1) and −120° (χ_2) is found in the complex with *syn*-TZ2PA6.[73] Overall, this analysis stresses the conformational plasticity of Trp286 and its capability to adopt different orientations depending on the chemical features of the ligand.

On the basis of the preceding discussion, the binding modes of **20**, **25**, and **27** were investigated using three models of hAChE, in which Trp286 was imposed to adopt each one of the three above-mentioned conformational orientations (denoted as A, B, and C; Figure 1). Moreover, suitable restraints were introduced to fix the orientation of the 6-chlorotacrine moiety, thus enhancing the conformational sampling of the ligand at the peripheral binding site and along the gorge. Noteworthy, this restrained docking protocol was able to predict the X-ray binding mode of bis(5)-tacrine, bis(7)-tacrine, tacrine(8)-4-aminoquinoline, (*R*)- and (*S*)-tacrine(10)-hupyridone, and *syn*- and *anti*-TZ2PA6 within the first 10 poses and with root-mean square deviations less than 1.8 Å (Table S3, Supporting Information).

Following previous studies in the literature,[79−81] the relative stabilities of the first 50 poses obtained in the docking of every ligand on each one of the targets were reranked using MM−PBSA calculations (Table S4, Supporting Information). In all cases the most favorable binding is found for target C, as this binding mode is favored by 4.3−7.6 and 2.4−9.9 kcal/mol when dielectric permittivities of 2 and 4 are considered for the interior of the ligand−hAChE complex, respectively, relative to the second most stable complex. Moreover, the results also show that there are small differences in the affinities estimated for the binding of hybrids **20**, **25**, and **27** to target C. Keeping in mind the range of uncertainty expected for MM−PBSA calculations,[80,82] this finding is in agreement with the similar inhibitory potencies measured for these compounds (IC_{50} values ranging from 7 to 14 nM, Table 1).

Inspection of the best poses found for hybrid **20** bound to target C shows that the 6-chlorotacrine moiety roughly matches the tacrine unit of *syn*-TZ2PA6. The slight

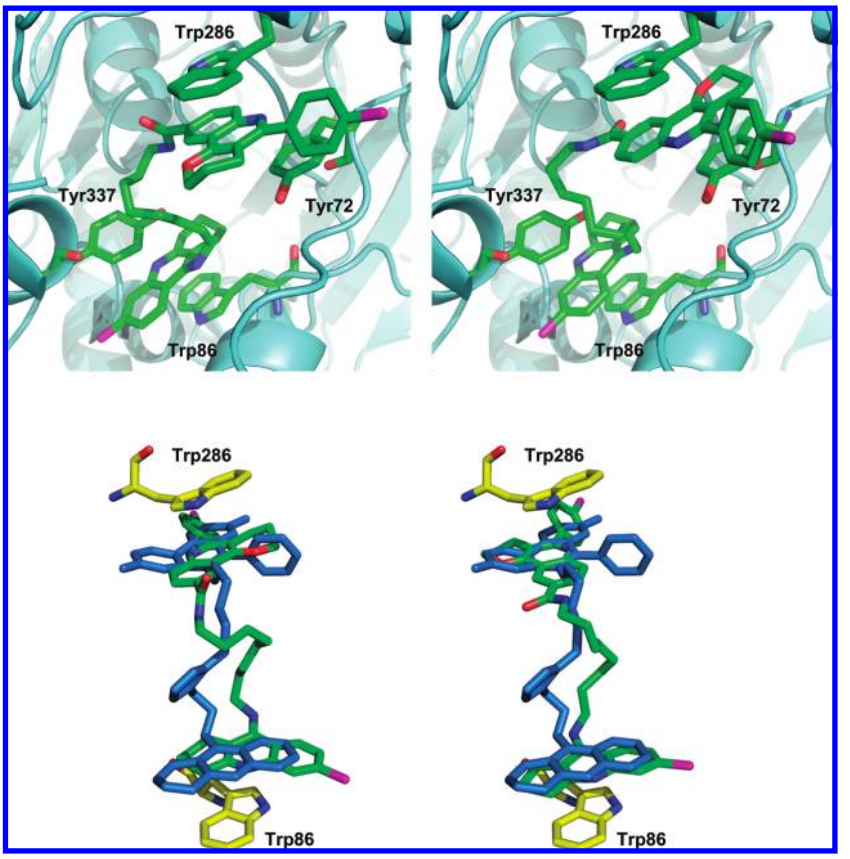

Figure 2. (Top) Representation of the most favorable binding mode of hybrid **20** (colored by atom) determined from MM-PBSA computations performed with internal permittivities of 2 (left) and 4 (right). Relevant residues at the catalytic (Trp86 and Tyr337) and peripheral (Trp286 and Tyr72) binding sites are colored by atom. (Bottom) Representation of the poses predicted for hybrid **20** from MM-PBSA computations and the orientation of *syn*-TZ2PA6 (blue) in the X-ray crystallographic structure of mouse AChE (PDB entry 1Q83).

displacement observed for the tetrahydroacridine systems can be ascribed to the positioning of the chlorine atom in **20** in the hydrophobic pocket formed by Trp439, Met443, and Pro446 (see above) and particularly to the active role played by the triazole ring in the tether of *syn*-TZ2PA6 in mediating interactions with specific residues along the gorge (see Figure 2),[73] which also explain the different arrangement of the linker observed for *syn*-TZ2PA6 and for the two poses of **20**. At the peripheral binding site the pyrano[3,2-*c*]-quinoline moiety adopts two main orientations (Figure 2), which can be roughly interconverted by a 180° rotation through the C5−C9 axis. At first sight, this finding might be surprising, keeping in mind the well-defined arrangement observed for the phenanthridinium moiety of *syn*-TZ2PA6 in the X-ray structure,[73] but this can be ascribed to additional interactions involving the buried phenanthridinium amino group that are absent in the case of the pyrano[3,2-*c*]-quinoline moiety. Accordingly, the stacking of the pyrano-[3,2-*c*]quinoline moiety might involve distinct arrangements provided that there exists a significant overlap with the aromatic rings of Trp286 and Tyr72 and that steric clashes with neighboring residues are avoided. Similar overall arrangements are found for hybrids **25** and **27** (see Figures S2 and S3, Supporting Information).

To further explore the proposed binding mode, a series of 10 ns molecular dynamics simulations were run for compounds **20** and **25**, which were chosen as representative members of the two series of dual binding site inhibitors. The simulations were run for each of the two potential binding modes shown in Figure 2 for compound **20** (and Figures S2 and S3 for **25**). Only the trajectories run for the ligand with the pyran ring oriented toward the bulk solvent yielded stable trajectories, as noted by inspection of the time dependence of both the potential energy and the root-mean-square deviation of selected atoms in the protein backbone, the binding site, and the ligand in the ligand−receptor complexes (Figure S4, Supporting Information). There is a large resemblance between the snapshots collected at the end of the trajectories and those used as starting structures (Figure 3). The main difference lies in the orientation of the tether, which adopts a more extended conformation at the end of the trajectories. Nevertheless, the tacrine unit remains stacked between the aromatic rings of Trp86 and Tyr337, and the pyrano[3,2-*c*]quinoline unit retains the $\pi-\pi$ stacking with Trp286 and Tyr72. Finally, a well-defined interaction pattern between the amido functionality and residues lining the entrance of the gorge is not observed. This finding is in contrast with the binding mode reported from modeling studies for a series of structurally related indole−tacrine hybrids containing an amido group within the linker,[23] where this group was proposed to participate in hydrogen-bond interactions with several residues in the gorge. These distinct features could presumably stem from the different arrangement of the pyrano[3,2-*c*]quinoline and indole units at the peripheral binding site.

Kinetic Analysis of AChE Inhibition. The mechanism of AChE inhibition was investigated in vitro using compound **20**, the most potent inhibitor of the two series. Graphical

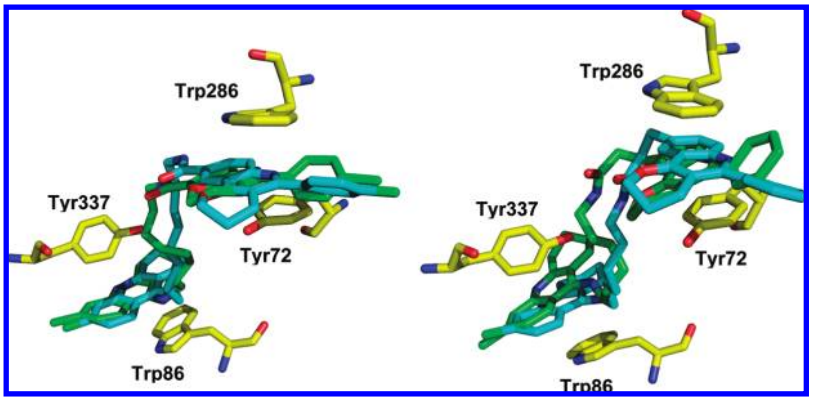

Figure 3. Representation of the structures (blue) collected at the end of the 10 ns molecular dynamics simulations of compounds **20** (left) and **25** (right) bound to AChE showing the stacking of the tacrine moiety with Trp86 and Tyr337 and of the phenylpyrano[3,2-*c*]quinoline unit with Trp286 and Tyr72 (yellow). The starting structure used in molecular dynamics simulations is shown in green.

analysis of the overlaid reciprocal Lineweaver−Burk plots (Figure 4) showed both increasing slopes (decreased V_{max}) and increasing intercepts (higher K_m) at increasing inhibitor concentration. This pattern indicates mixed-type inhibition. Therefore, in agreement with molecular modeling studies, the pattern in Figure 4 shows that **20** is able to bind the peripheral site as well as the active site of hAChE. Replots of the slope versus concentration of **20** give an estimate of the competitive inhibition constant, K_i, of 1.91 nM.

BChE Inhibition. Recent evidence has shown that inhibition of BChE might be valuable in the search for anti-Alzheimer agents.[83,84] Consequently, the inhibitory activity on human serum BChE (hBChE) was also assayed by the method of Ellman et al. (Table 1).[64] 6-Chlorotacrine inhibits hAChE 110-fold more potently than hBChE.[31] The presence of the chlorine atom at the tacrine unit, which leads to an increased AChE inhibitory activity relative to unsubstituted tacrine,[85−87] becomes detrimental for hBChE inhibition. A steric hindrance due to the proximity of the chlorine atom to the terminal methyl group of Met437 in the hBChE active site seems to account for the detrimental influence of this substituent on the hBChE inhibitory activity relative to tacrine,[23,65] which is 21-fold more potent toward hBChE than 6-chlorotacrine.[31] As expected, hybrids **18**−**27** are more potent inhibitors of hAChE than hBChE (32- to 106-fold and 16- to 77-fold in the first and second series, respectively). Hybrids **23**−**27** exhibit IC_{50} values in the nanomolar range, they being 1.5- to 7-fold more potent than their counterparts of the first series and up to 3- to 4-fold more potent than 6-chlorotacrine.

Inhibition of Aβ Aggregation and Formation. Inhibition of AChE-Induced Aβ Aggregation. With the design of this novel family of dual binding site AChEIs, an interference with the AChE-induced Aβ aggregation was also pursued. Thus, the new hybrids were tested for their ability to inhibit the AChE-induced aggregation of $A\beta_{1-40}$, by using a thioflavin T fluorescence method.[88] Also, the Aβ-antiaggregating effect of one of the tricyclic ester precursors, **12**, was determined, while those of propidium[88] and 6-chlorotacrine[31] were already described. The new hybrids significantly inhibit, at 100 μM, the hAChE-induced Aβ aggregation, with percentages of inhibition ranging from 23% to 46% (Table 2), while 6-chlorotacrine and **12** were the almost inactive. Most of the new hybrids could be classified as weak inhibitors of the AChE-induced Aβ aggregation, with expected IC_{50} values in the high micromolar range, while the most potent described inhibitors display potencies in the low micromolar range.[21,23,26,27,30,33] Nevertheless, the inhibitory activity of the most potent hybrids, **26** and **27**, is in the same range as that of other known dual binding site AChEIs.[20,22,24,28,29,31,32]

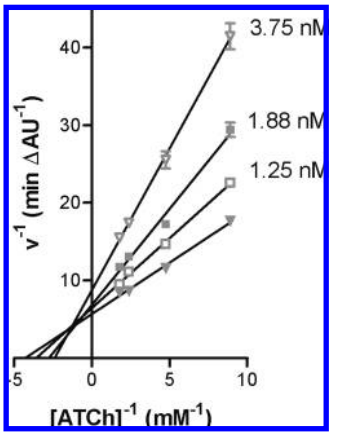

Figure 4. Kinetic study on the mechanism of AChE inhibition by **20**. Overlaid Lineweaver−Burk reciprocal plots of AChE initial velocity at increasing substrate concentration (ATCh, 0.56−0.11 mM) in the absence of inhibitor and in the presence of **20** (1.25−3.75 nM) are shown. Lines were derived from a weighted least-squares analysis of the data points.

The Aβ antiaggregating effect of the novel hybrids seems to depend on the position of the amido group within the linker, the hybrids of the second series being more potent than their counterparts of the first series. Moreover, the Aβ antiaggregating effect seems to be independent of the length of the linker within the first series, while a slightly increased effect is observed upon lengthening of the linker in the second series. Overall, the most potent AChE-induced Aβ aggregation inhibitors within both series were hybrids **26** and **27**. The higher Aβ antiaggregating activity of the novel hybrids relative to 6-chlorotacrine and **12** seems to be indicative of their dual binding site character. In turn, their lower Aβ antiaggregating activity relative to propidium could be ascribed to the different binding mode of the pyrano[3,2-*c*]quinoline moiety of these hybrids at the AChE peripheral site and/or to a less efficient interaction with Trp286 due to the lack of cation−π interaction in our hybrids, which are not protonated at the quinoline nitrogen atom of this moiety at physiological pH.

Table 2. Aβ Aggregation and BACE-1 Inhibitory Activities of the Hydrochlorides of 6-Chlorotacrine and Tricyclic Ester **12**, Propidium Iodide, and the Dihydrochlorides of the Pyrano[3,2-*c*]quinoline−6-Chlorotacrine Hybrids[a]

compd	AChE-induced $A\beta_{1-40}$ aggregation[b] (%)	$A\beta_{1-42}$ self-induced aggregation[c] (%)	BACE-1 activity[d] (%)
18·2HCl	27.2 ± 7.1	16.4 ± 2.6	na[e]
19·2HCl	22.9 ± 3.2	28.6 ± 3.3	14.5 ± 5.7
20·2HCl	28.6 ± 0.5	21.5 ± 1.8	18.5 ± 7.6
21·2HCl	nd[f]	nd[f]	nd[f]
22·2HCl	27.9 ± 5.2	20.5 ± 1.1	na[e]
23·2HCl	34.4 ± 1.0	45.3 ± 0.9	na[e]
24·2HCl	37.9 ± 3.4	12.2 ± 1.1	na[e]
25·2HCl	38.9 ± 2.6	30.8 ± 8.6	19.6 ± 5.1
26·2HCl	45.9 ± 2.8	49.1 ± 15.1	34.4 ± 3.6
27·2HCl	45.7 ± 0.3	47.3 ± 8.8	77.8 ± 6.4
12·HCl	10.5 ± 4.7	na[e]	na[e]
propidium iodide	82.0 ± 2.5[g]	89.8 ± 0.9	nd[f]
6-chlorotacrine·HCl	8.5 ± 1.6[h]	7.1 ± 1.2	na[e]

[a] Values are expressed as mean ± standard error of the mean from two independent measurements, each performed in duplicate. [b] A 100 μM concentration of the inhibitor was used. [c] A 50 μM concentration of the inhibitor was used ([Aβ]/[I] = 1/1). [d] A 2.5 μM concentration of the inhibitor was used. [e] Not active. [f] Not determined. [g] Data from ref 88. [h] Data from ref 31.

Inhibition of Spontaneous Aβ Aggregation. A number of dual binding site AChE inhibitors exhibit a significant inhibitory activity on Aβ self-aggregation.[23,26,27,29,32−34] The new hybrids significantly inhibit the self-induced Aβ aggregation when tested at equimolar ratio with Aβ, with percentages of inhibition ranging from 12% to 49% (Table 2). In the same assay conditions, 6-chlorotacrine and the tricyclic ester **12** turned out to be, respectively, almost and completely inactive, while propidium was more potent than the new hybrids. Hybrids of the second series were generally more potent than their counterparts of the first series, with the sole exception of **24** which was 2-fold less potent than **19**. A clear dependency of the spontaneous Aβ antiaggregating activity on the length of the linker was not observed. Compounds **23**, **26**, and **27** were the most potent hybrids. It might be hypothesized that a two-methylene linker between the amido group and the phenylpirano[3,2-*c*]quinoline moiety facilitates the formation of hydrogen bonds, with Aβ leading to an increased affinity. The expected IC_{50} values for the most potent hybrids must be around 50 μM, while the strongest inhibitors of spontaneous Aβ aggregation among known dual binding site AChEIs show potencies in the low micromolar range.[26,27,33,34] Thus, **23**, **26**, and **27** can be considered moderate inhibitors of $A\beta_{1-42}$ self-aggregation.

Inhibition of BACE-1. BACE-1 has been largely investigated as a therapeutic target for disease-modifying agents in AD, since BACE-1 is involved in the proteolytic cleavage of APP to Aβ and BACE-1 knockout mice did not show any adverse phenotype. Although highly active in vitro peptide inhibitors with poor pharmacokinetics are known, potent brain permeable inhibitors have not been developed yet. Therefore, there is an increasing need for small organic BACE-1 inhibitors able to cross the BBB.[89] The ability of the novel hybrids to inhibit in vitro human recombinant BACE-1 was also investigated. Some dual binding site AChEIs such as donepezil,[90] bis(7)-tacrine,[91] lipocrine,[92] memoquin,[26] and AP2243[93] exhibit BACE-1 inhibitory activity, which increases their potential as disease-modifying anti-Alzheimer drug candidates. In particular, since the new hybrids might structurally resemble to some extent bis(7)-tacrine, which showed in vitro and in vivo activity,[91] their BACE-1 inhibitory activity was first screened at a single concentration (2.5 μM) by a fluorometric assay.[94]

Hybrid **27** was the most potent BACE-1 inhibitor, exhibiting a 78% inhibition. Compounds **19**, **20**, **25**, and **26** were less active than **27** (15−34% inhibition), and the rest of the hybrids, the tricyclic ester **12**, and 6-chlorotacrine were inactive (Table 2). In general the BACE-1 inhibitory activity of the hybrids of the second series was higher than that of their counterparts of the first series. For the second series, the inhibitory activity increased along with the tether length. The IC_{50} value of the most active hybrid (**27**) was 1.81 ± 0.48 μM, it being more active than bis(7)-tacrine in vitro (IC_{50} = 7.5 μM).[91] Thus, **27** emerged as a promising anti-Alzheimer drug candidate endowed with a potent hAChE inhibitory activity (nanomolar range) and a significant in vitro inhibitory effect on both Aβ formation and AChE-induced and self-induced Aβ aggregation.

In Vitro Blood−Brain Barrier Permeation Assay. Brain penetration is a major issue for successful CNS drugs. In the past years, several in silico/in vitro methods have been used to predict the BBB permeation potential of test compounds. Among them, the parallel artificial membrane permeation assay (PAMPA-BBB) described by Di et al.[95] predicts passive BBB permeation with high success, high throughput, and reproducibility. To evaluate the brain penetration of the pyrano[3,2-*c*]quinoline−6-chlorotacrine hybrids herein described, we used the PAMPA-BBB assay, which was successfully applied by some of us to different compounds.[39,52,96−98] The in vitro permeability (P_e) of selected hybrids (**18**, **19**, and **23**−**27**), the tricyclic ester **12**, and 6-chlorotacrine through a lipid extract of porcine brain was determined by using phosphate buffered saline (PBS)/EtOH (80:20 or 70:30, depending on the solubility of compounds). At each solvent mixture, assay validation was made by comparing the experimental permeability with the reported values of 15 commercial drugs that gave a good lineal correlation: $P_e(\text{exp}) = 1.48P_e(\text{bibl}) + 1.91$ ($R^2 = 0.95$) for PBS/EtOH (80:20) and $P_e(\text{exp}) = 1.99\ P_e(\text{bibl}) + 1.07$ ($R^2 = 0.92$) for PBS/EtOH (70:30). From these equations and taking into account the limits established by Di et al. for BBB permeation,[95] we established that compounds with permeability values over 7.8×10^{-6} cm s^{-1} (PBS/EtOH, 80:20) or 9.0×10^{-6} cm s^{-1} (PBS/EtOH, 70:30) should cross the BBB. All tested hybrids showed permeability values over the above limits (Table 3; see also Table S5, Supporting Information), pointing out that they could cross the BBB and reach their pharmacological targets located in the CNS.

Table 3. Permeability Results from the PAMPA-BBB Assay for Selected Pyrano[3,2-*c*]quinoline−6-Chlorotacrine Hybrids (P_e, 10^{-6} cm s^{-1}) with Their Predictive Penetration into the CNS

compd	P_e (10^{-6} cm s^{-1})[a]	prediction
18·2HCl[b]	14.9 ± 1.1	CNS+
19·2HCl[b]	17.7 ± 0.2	CNS+
23·2HCl[c]	15.1 ± 0.2	CNS+
24·2HCl[b]	10.6 ± 0.4	CNS+
25·2HCl[c]	13.2 ± 0.4	CNS+
26·2HCl[b]	10.2 ± 0.3	CNS+
27·2HCl[b]	10.1 ± 0.4	CNS+
12[c]	21.4 ± 0.6	CNS+
6-chlorotacrine·HCl[c]	19.8 ± 0.4	CNS+

[a] Values are expressed as the mean ± standard deviation of three independent experiments. [b] Compound dissolved in PBS/EtOH (70:30). [c] Compound dissolved in PBS/EtOH (80:20).

Conclusion

We have synthesized a new series of pyrano[3,2-*c*]-quinoline−6-chlorotacrine hybrids as a novel class of dual binding site AChEIs. Variation of the position of an amido group within the oligomethylene linker gives rise to two parallel isomeric series. In general, the new hybrids are potent AChEIs, with IC_{50} values in the low nanomolar range and with slight differences between both series. The results indicate that linkage of a 5-phenylpyrano[3,2-*c*]quinoline moiety to a unit of the highly potent AChE active site inhibitor 6-chlorotacrine through an amido-containing tether does not result in an increased potency, as the most potent hybrids are equipotent to 6-chlorotacrine. Moreover, the AChE inhibitory potency of the hybrids shows a modest dependence on the length of the linker and the position of the amido group. Molecular modeling and kinetic studies have confirmed the dual site binding of these hybrids to hAChE. Apart from the characteristic interactions of the 6-chlorotacrine unit of these hybrids within the active site of AChE, the pyranoquinoline moiety is proposed to interact at the peripheral site forming a double near-parallel stacking with Trp286 and Tyr72, respectively, which are positioned in a way similar to the arrangement found in the complex of the enzyme with *syn*-TZ2PA6. The presence of a chlorine atom at position 6 of the tacrine unit, known to be detrimental for BChE inhibition, not unexpectedly accounts for the hAChE/hBChE selectivity of these hybrids.

Because of their dual binding site character, the new hybrids are able to inhibit the AChE-induced Aβ_{1-40} aggregation. Also, these compounds exhibit a significant ability to inhibit the self-induced Aβ_{1-42} aggregation, and some of them can also inhibit BACE-1. In general, these effects seem to be sensitive to the position of the amido group of the linker, the hybrids of the second series being more potent than their counterparts of the first series. Moreover, in the second series the activities increase along with the tether length. Finally, these hybrids seem to be able to cross BBB. Overall, **27** emerges as a promising anti-Alzheimer drug candidate able to hit both AChE (catalytic and noncatalytic activities) and Aβ (aggregation and production) and, therefore, with potential symptomatic and disease-modifying effects.

Experimental Section

Chemistry. General Methods. Melting points were determined in open capillary tubes with a MFB 595010M Gallenkamp or a Büchi B-540 melting point apparatus. 300 MHz ^{1}H/75.4 MHz ^{13}C NMR spectra, 400 MHz ^{1}H/100.6 MHz ^{13}C NMR spectra, and 500 MHz ^{1}H NMR spectra were recorded on Varian Gemini 300, Varian Mercury 400, and Varian Inova 500 spectrometers, respectively. The chemical shifts are reported in ppm (δ scale) relative to internal tetramethylsilane, and coupling constants are reported in hertz (Hz). Assignments given for the NMR spectra of the new compounds have been carried out by comparison with the NMR data of **18**, **27**, and 6-chlorotacrine, as model compounds, which in turn were assigned on the basis of DEPT, COSY ^{1}H/^{1}H (standard procedures), and COSY ^{1}H/^{13}C (gHSQC and gHMBC sequences) experiments. IR spectra were run on Perkin-Elmer Spectrum RX I or Thermo Nicolet Nexus spectrophotometers. Absorption values are expressed as wavenumbers (cm^{-1}); only significant absorption bands are given. Column chromatography was performed on silica gel 60 AC.C (35−70 mesh, SDS, ref 2000027). Thin-layer chromatography was performed with aluminum-backed sheets with silica gel 60 F_{254} (Merck, ref 1.05554), and spots were visualized with UV light and 1% aqueous solution of $KMnO_4$. The analytical samples of all of the new hybrids that were subjected to pharmacological evaluation possess a purity of ≥95%, as evidenced by results of their elemental analyses.

(4a*RS*,5*RS*,10b*RS*)- and (4a*RS*,5*SR*,10b*RS*)-Ethyl 5-(4-Chlorophenyl)-3,4,4a,5,6,10b-hexahydro-2*H*-pyrano[3,2-*c*]quinoline-9-carboxylate (9). $Y(OTf)_3$ (295 mg, 0.55 mmol, 0.2 equiv) was added to a solution of *p*-chlorobenzaldehyde, **7** (385 mg, 2.74 mmol, 1 equiv), and ethyl *p*-aminobenzoate, **5** (453 mg, 2.74 mmol, 1 equiv), in dry CH_3CN (20 mL). A solution of 3,4-dihydro-2*H*-pyran, **4** (250 μL, 231 mg, 2.74 mmol, 1 equiv), in dry CH_3CN (3 mL) was then added, and the reaction mixture was stirred at room temperature under inert atmosphere for 12 h. Saturated aqueous $NaHCO_3$ (20 mL) was added, and the resulting mixture was extracted with AcOEt (3 × 10 mL). The combined organic extracts were dried with anhydrous Na_2SO_4, filtered, and concentrated under reduced pressure to give a residue (1.1 g), which was subjected to column chromatography [35−70 μm silica gel (40 g), hexane/AcOEt mixtures]. On elution with hexane/AcOEt, 20:80, the desired product **9** (722 mg, 71% yield) was isolated as a 1.3:1 mixture of diastereoisomers as a waxy solid. A single diastereoisomer was obtained as a waxy solid in pure form from fractions isolated from the flash chromatography (51 mg, 5% yield) and characterized as the all-cis isomer (4a*RS*,5*RS*,10b*RS*): IR (NaCl) ν 3346 (N−H st), 1685 (C=O st) cm^{-1}; ^{1}H NMR (400 MHz, $CDCl_3$) δ 1.27−1.62 (m, 4H, 3-H_2 and 4-H_2), 1.37 (t, J = 7.1 Hz, 3H, CH_2-CH_3), 2.16 (m, 1H, 4a-H), 3.43 (dt, J = 12.0, J' = 1.9 Hz, 1H, 2-H_{ax}), 3.63 (broad d, $J \approx$ 12.0 Hz, 1H, 2-H_{eq}), 4.26 (s, 1H, NH), 4.33 (m, 2H, CH_2-CH_3), 4.73 (d, J = 1.7 Hz, 1H, 10b-H), 5.28 (d, J = 5.4 Hz, 1H, 5-H), 6.58 (d, J = 8.4 Hz, 1H, 7-H), 7.30−7.40 (complex signal, 4H, 5-ArH), 7.79 (d, J = 8.4 Hz, 1H, 8-H), 8.11 (s, 1H, 10-H); ^{13}C NMR (100.6 MHz, $CDCl_3$) δ 14.5 (CH_3, CH_2-CH_3), 18.1 (CH_2, C3), 25.3 (CH_2, C4), 38.4 (CH, C4a), 58.6 (CH, C5), 60.3 (CH_2, CH_2-CH_3), 60.7 (CH_2, C2), 72.1 (CH, C10b), 113.6 (CH, C7), 118.7 (C, C9), 120.3 (C, C10a), 128.0 (CH, C8), 128.7 (CH, 5-Ar-C_{meta}), 129.8 (CH, 5-Ar-C_{ortho}), 130.1 (CH, C10), 133.5 (C, 5-Ar-C_{para}), 138.7 (C, 5-Ar-C_{ipso}), 148.7 (C, C7a), 166.8 (C, CO). HRMS calcd for (C_{21}-$H_{22}{}^{35}ClNO_3$ + H^+) 372.1361, found 372.1370.

Ethyl 5-(4-Chlorophenyl)-3,4-dihydro-2*H*-pyrano[3,2-*c*]quinoline-9-carboxylate (11). To a solution of the diastereomeric mixture of tetrahydroquinolines **9** (408 mg, 1.11 mmol) in $CHCl_3$ (15 mL), DDQ (498 mg, 2.19 mmol, 2 equiv) was added, and the reaction mixture was stirred at room temperature for 24 h. Saturated aqueous Na_2CO_3 (50 mL) was added, the organic phase was separated, and the aqueous one was extracted with CH_2Cl_2 (3 × 10 mL). The combined organic phase and extracts were dried with anhydrous Na_2SO_4 and evaporated under reduced pressure to give a crude residue (870 mg), which was subjected to column chromatography [35−70 μm silica gel (20 g), hexane/AcOEt mixtures]. On elution with hexane/AcOEt, 50:50, pyranoquinoline **11** (305 mg, 75% yield) was obtained as an off-white solid: mp 197−199 °C (hexane/AcOEt, 1:1); IR (NaCl) ν 1715 (C=O st), 1623 (ar−C−C and ar−C−N st) cm^{-1}; ^{1}H NMR (400 MHz, CD_3OD) δ 1.36 (t, J = 7.1 Hz, 3H, CH_2-CH_3),

2.09 (m, 2H, 3-H_2), 2.76 (t, J = 6.3 Hz, 2H, 4-H_2), 4.39 (q, J = 7.1 Hz, 2H, CH_2-CH_3), 4.60 (m, 2H, 2-H_2), 7.60−7.70 (complex signal, 4H, 5-ArH), 8.04 (dd, J = 8.9 Hz, J' = 0.5 Hz, 1H, 7-H), 8.46 (dd, J = 8.9 Hz, J' = 1.8 Hz, 1H, 8-H), 8.93 (dd, J = 1.8 Hz, J' = 0.5 Hz, 1H, 10-H); ^{13}C NMR (100.6 MHz, CD_3OD) δ 13.4 (CH_3, CH_2-CH_3), 20.3 (CH_2, C3), 22.3 (CH_2, C4), 62.0 (CH_2, CH_2−CH_3), 70.3 (CH_2, C2), 114.5 (C, C4a), 119.3 (C, C10a), 120.8 (CH, C10), 125.1 (C, C9), 129.4 (CH, C7), 130.1 (CH, C8), 130.3 (CH, 5-Ar-C_{ortho}), 130.8 (CH, 5-Ar-C_{meta}), 133.3 (C, 5-Ar-C_{para}), 138.0 (C, 5-Ar-C_{ipso}), 140.6 (C, C6a), 157.2 (C, C10b), 165.0 (C, C5), 166.3 (C, CO). HRMS calcd for ($C_{21}H_{18}{}^{35}ClNO_3 + H^+$) 368.1048, found 368.1056.

Methyl 3-(3,4-Dihydro-5-phenyl-2*H*-pyrano[3,2-*c*]quinolin-9-yl)propanoate (12). A. Synthesis of the Diastereomeric Mixture of Tetrahydroquinolines 10. To a solution of 3,4-dihydro-2*H*-pyran (508 μL, 468 mg, 5.58 mmol, 1 equiv), benzaldehyde (566 μL, 591 mg, 5.58 mmol, 1 equiv), and the aniline **6** (1.00 g, 5.58 mmol, 1 equiv) in CH_3CN (40 mL) was added $Sc(OTf)_3$ (550 mg, 1.12 mmol, 0.2 equiv), and the reaction mixture was stirred overnight under inert atmosphere at room temperature. Saturated aqueous $NaHCO_3$ (40 mL) was added, and the resulting mixture was extracted with AcOEt (3 × 30 mL). The combined organic extracts were dried with anhydrous $MgSO_4$ and concentrated under reduced pressure to give a residue (1.9 g), which was subjected to column chromatography [35−70 μm silica gel (40 g), hexane/AcOEt/Et_3N mixtures]. On elution with hexane/AcOEt/Et_3N, 74:25:1, the expected adduct **10** (1.68 g, 86% yield) was obtained as a diastereomeric mixture.

B. DDQ Oxidation of 10 to 12: Overoxidation of 12 to Its Cinnamic Derivative. To a solution of the mixture of diastereoisomers **10** (4.75 g, 13.5 mmol, 1 equiv) in $CHCl_3$ (50 mL) were added Et_3N (5.70 mL, 4.14 g, 40.8 mmol, 3 equiv) and DDQ (3.10 g, 13.6 mmol, 1 equiv). The reaction mixture was heated to reflux for 3 h and concentrated in vacuo. The resulting solid residue (7.90 g) was subjected to column chromatography [35−70 μm silica gel (200 g), hexane/AcOEt mixtures]. On elution with hexane/AcOEt, 20:80, the desired pyranoquinoline **12** (1.60 g) was obtained together with its cinnamic derivative (1.60 g, 35% combined yield).

C. Hydrogenation of the Mixture of 12 and Its Cinnamic Derivative. The previous mixture (100 mg) was subjected to hydrogenation at atmospheric pressure in EtOH (10 mL) in the presence of 10% w/w Pd/C (20 mg) for 12 h. The resulting mixture was filtered, and the filtrate was concentrated in vacuo. The resulting residue was taken up in AcOEt (15 mL) and washed with saturated aqueous $NaHCO_3$ (20 mL), and the organic phase was dried with anhydrous $MgSO_4$ and evaporated at reduced pressure to yield the desired pyranoquinoline **12** (98 mg, 95% overall yield from **10**), which was obtained as a glassy white solid: mp 93−94 °C (AcOEt); IR (NaCl) ν 1736 (C=O st) cm^{-1}; ^{1}H NMR (400 MHz, $CDCl_3$) δ 1.99 (m, 2H, 3-H_2), 2.73 (complex signal, 4H, 4-H_2 and 9-CH_2-CH_2-COO), 3.13 (t, J = 7.8 Hz, 2H, 9-CH_2-CH_2-COO), 3.67 (s, 3H, $COOCH_3$), 4.42 (t, J = 5.2 Hz, 2H, 2-H_2), 7.43 (complex signal, 4H, 8-H, 5-ArH_{meta}, and 5-ArH_{para}), 7.55 (dd, J = 8.4 Hz, J' = 1.5 Hz, 2H, 5-ArH_{ortho}), 7.94 (d, J = 1.5 Hz, 1H, 10-H), 7.97 (d, J = 8.4 Hz, 1H, 7-H); ^{13}C NMR (100.6 MHz, $CDCl_3$) δ 21.7 (CH_2, C3), 23.6 (CH_2, C4), 31.0 (CH_2, 9-CH_2-CH_2-COO), 35.5 (CH_2, 9-CH_2-CH_2-COO), 51.5 (CH_3, COOCH_3), 66.9 (CH_2, C2), 110.6 (C, C4a), 119.6 (C, C10a), 119.7 (CH, C10), 128.0 (CH, C7), 128.1 (CH, 5-Ar-C_{para}), 128.6 (CH, 5-Ar-C_{ortho}), 129.0 (CH, 5-Ar-C_{meta}), 130.1 (CH, C8), 137.5 (C, C9), 140.3 (C, 5-Ar-C_{ipso}), 146.0 (C, C6a), 156.9 (C, C10b), 160.2 (C, C5), 173.1 (C, COO). HRMS calcd for ($C_{22}H_{21}NO_3 + H^+$) 348.1594, found 348.1588.

General Procedure for the Reaction of 6,9-Dichloro-1,2,3,4-tetrahydroacridine, 15, with α,ω-Alkanediamines. A mixture of **15** (1 mmol) and an excess of the diamine **16** (4 mmol) in 1-pentanol (1.3 mL) was heated under reflux with magnetic stirring for 18 h. The resulting mixture was cooled to room temperature, diluted with CH_2Cl_2 (3 mL), and washed successively with aqueous 2 N NaOH (3 × 3 mL) and water (2 × 3 mL). The organic phase was dried with anhydrous Na_2SO_4 and concentrated in vacuo to give a brown oily residue, from which 1-pentanol and the excess of diamine were removed by distillation at 100 °C/1 Torr and 140 °C/1 Torr, respectively. The distillation residue was taken in CH_2Cl_2 (1.3 mL), filtered, and concentrated in vacuo to give a brown oily residue which was subjected to column chromatography (35−70 μm silica gel, CH_2Cl_2/MeOH/25% or 50% aqueous NH_4OH or AcOEt/MeOH/Et_3N mixtures as eluent) to afford, separately, bis-6-chlorotacrine **28** and the desired amine **17** as a brown and yellowish oil, respectively.

For characterization purposes, analytical samples of the dihydrochlorides of **17** and **28** were prepared as follows: the amine **17** or the dimer **28** (1 mmol) were dissolved in MeOH (2−10 mL), the solution was filtered through a polytetrafluoroethylene (PTFE) 0.45 μm filter and treated with an excess of a methanolic solution of HCl (6−9 mmol), and the resulting solution was concentrated in vacuo to dryness. The solid was recrystallized from MeOH/AcOEt mixtures, triturated with Et_2O, and dried at 65 °C/15 Torr for 4 days to give **17**·2HCl or **28**·2HCl as yellowish solids.

9-[(6-Aminohexyl)amino]-6-chloro-1,2,3,4-tetrahydroacridine Dihydrochloride (17c·2HCl). From **15** (4.00 g, 15.9 mmol) and 1,6-diaminohexane, **16c** (7.52 g, 64.8 mmol), a brown oily residue (7.30 g) was obtained and subjected to column chromatography [35−70 μm silica gel (88 g), CH_2Cl_2/MeOH/25% aqueous NH_4OH mixtures]. On elution with CH_2Cl_2/MeOH/25% aqueous NH_4OH, 99:1:0.05, bis(6)-6-chlorotacrine, **28c** (246 mg), a mixture **28c**/**17c** in the approximate ratio of 20:80 (^{1}H NMR) (614 mg, 8% total yield of **28c**), and amine **17c** (3.61 g, 78% total yield) were consecutively isolated as brown-yellow oils: $R_{f(\mathbf{17c})}$ = 0.39; $R_{f(\mathbf{28c})}$ = 0.80 (CH_2Cl_2/MeOH/25% aqueous NH_4OH, 9:1:0.01).

17c·2HCl: mp 157−158 °C (MeOH); IR (KBr) ν 3500−2500 (max at 3413, 2935, 2864, N−H, $^+$N−H, and C−H st), 1630, 1573, and 1513 (ar−C−C and ar−C−N st) cm^{-1}; ^{1}H NMR (300 MHz, CD_3OD, presat/Watergate) δ 1.39−1.52 (complex signal, 4H, 3′-H_2 and 4′-H_2), 1.66 (tt, $J \approx J' \approx$ 7.5 Hz, 2H, 5′-H_2), 1.80 (tt, $J \approx J' \approx$ 7.5 Hz, 2H, 2′-H_2), 1.88−1.98 (complex signal, 4H, 2-H_2 and 3-H_2), 2.69 (m, 2H, 1-H_2), 2.90 (t, J = 7.5 Hz, 2H, 6′-H_2), 2.98 (m, 2H, 4-H_2), 3.83 (t, J = 7.5 Hz, 2H, 1′-H_2), 7.48 (dd, J = 9.3 Hz, J' = 2.1 Hz, 1H, 7-H), 7.75 (d, J = 2.1 Hz, 2H, 5-H), 8.30 (d, J = 9.3 Hz, 1H, 8-H); ^{13}C NMR (75.4 MHz, CD_3OD) δ 22.3 (CH_2, C3), 23.2 (CH_2, C2), 25.2 (CH_2, C1), 27.1 (CH_2) and 27.3 (CH_2) (C3′ and C4′), 28.5 (CH_2), 30.9 (CH_2) and 31.4 (CH_2) (C4, C2′, and C5′), 40.6 (CH_2, C6′), 49.1 (CH_2, C1′), 114.3 (C, C9a), 116.5 (C, C8a), 121.3 (CH, C5), 126.1 (CH, C7), 128.0 (CH, C8), 138.5 (C, C6), 142.8 (C, C10a), 154.5 (C, C4a), 156.2 (C, C9).

28c·2HCl [*N*,*N*′-Bis(6-chloro-1,2,3,4-tetrahydroacridin-9-yl)-1,6-hexanediamine]: mp 126−127 °C (MeOH); IR (KBr) ν 3500−2500 (max at 3254, 3049, 2933, 2859, 2792, N−H, $^+$N−H, and C−H st), 1631, 1603, 1574, 1557, and 1514 (ar−C−C and ar−C−N st) cm^{-1}; ^{1}H NMR (300 MHz, CD_3OD) δ 1.50 (m, 4H, 3′-H_2), 1.80−2.00 (complex signal, 12H, 2-H_2, 3-H_2, and 2′-H_2), 2.66 (m, 4H, 1-H_2), 2.98 (m, 4H, 4-H_2), 3.91 (t, $J \approx$ 7.0 Hz, 4H, 1′-H_2), 4.87 (s, NH and $^+$NH), 7.51 (dd, J = 9.6 Hz, J' = 2.2 Hz, 2H, 7-H), 7.75 (d, J = 2.2 Hz, 2H, 5-H), 8.35 (d, $J \approx$ 9.6 Hz, 2H, 8-H); ^{13}C NMR (75.4 MHz, CD_3OD) δ 22.5 (CH_2, C3), 23.3 (CH_2, C2), 25.3 (CH_2, C1), 27.4 (CH_2), 31.4 (CH_2), and 31.6 (CH_2) (C4, C2′, and C3′), 49.2 (CH_2, C1′), 114.6 (C, C9a), 116.9 (C, C8a), 122.1 (CH, C5), 125.9 (CH, C7), 127.7 (CH, C8), 138.0 (C, C6), 143.6 (C, C10a), 155.3 (C), and 155.6 (C) (C4a and C9).

9-[(8-Aminooctyl)amino]-6-chloro-1,2,3,4-tetrahydroacridine Dihydrochloride (17e·2HCl). From **15** (4.00 g, 15.9 mmol) and 1,8-diaminooctane, **16e** (8.24 g, 57.2 mmol), a brown oily residue (9.56 g) was obtained and subjected to column chromatography [35−70 μm silica gel (115 g), CH_2Cl_2/MeOH/25% aqueous NH_4OH mixtures]. On elution with CH_2Cl_2/MeOH/

25% aqueous NH_4OH, 96:4:0.1 to 85:15:0.2, bis(8)-6-chlorotacrine, **28e** (2.11 g, 46% yield) and amine **17e** (2.00 g, 35% yield) were consecutively isolated as brown-yellow oils: $R_{f(\mathbf{17e})} = 0.33$; $R_{f(\mathbf{28e})} = 0.88$ (CH_2Cl_2/MeOH/25% aqueous NH_4OH, 9:1:0.01).

17e·2HCl: mp 109−110 °C (MeOH/AcOEt, 1:1); IR (KBr) ν 3500−2500 (max at 3344, 2929, 2855, N−H, $^+$N−H, and C−H st), 1630, 1605, 1574, 1558, and 1512 (ar−C−C and ar−C−N st) cm^{-1}; ^{1}H NMR (300 MHz, CD_3OD) δ 1.24−1.44 (complex signal, 8H, 3′-H_2, 4′-H_2, 5′-H_2, and 6′-H_2), 1.63 (tt, $J \approx J' \approx 7.5$ Hz, 2H, 7′-H_2), 1.71 (tt, $J \approx J' \approx 7.5$ Hz, 2H, 2′-H_2), 1.84−1.94 (complex signal, 4H, 2-H_2 and 3-H_2), 2.66 (m, 2H, 1-H_2), 2.89 (t, $J = 7.5$ Hz, 2H, 8′-H_2), 2.94 (m, 2H, 4-H_2), 3.69 (t, $J = 7.5$ Hz, 2H, 1′-H_2), 4.89 (s, NH, $^+$NH and $^+NH_3$), 7.36 (dd, $J = 9.0$ Hz, $J' = 2.1$ Hz, 1H, 7-H), 7.71 (d, $J = 2.1$ Hz, 1H, 5-H), 8.16 (d, $J =$ 9.0 Hz, 1H, 8-H); ^{13}C NMR (75.4 MHz, CD_3OD) δ 22.8 (CH_2, C3), 23.5 (CH_2, C2), 25.5 (CH_2, C1), 27.4 (CH_2) and 27.7 (CH_2) (C3′ and C6′), 28.6 (CH_2), 30.1 (2 CH_2), 31.8 (CH_2), and 32.1 (CH_2) (C4, C2′, C4′, C5′, and C7′), 40.8 (CH_2, C8′), 49.4 (CH_2, C1′), 115.1 (C, C9a), 117.6 (C, C8a), 123.3 (CH, C5), 125.6 (CH, C7), 127.4 (CH, C8), 137.3 (C, C6), 144.9 (C, C10a), 155.0 (C, C4a), 156.6 (C, C9).

28e·2HCl [*N,N′*-Bis(6-chloro-1,2,3,4-tetrahydroacridin-9-yl)-1,8-octanediamine]: mp 134−135 °C (MeOH/AcOEt, 1:1); IR (KBr) ν 3500−2500 (max at 3229, 3046, 2926, 2853, 2768, N−H, $^+$N−H, and C−H st), 1630, 1570, and 1515 (ar−C−C and ar−C−N st) cm^{-1}; ^{1}H NMR (300 MHz, CD_3OD, presat/Watergate) δ 1.37−1.48 (complex signal, 8H, 3′-H_2 and 4′-H_2), 1.83 (tt, $J \approx J' \approx 7.2$ Hz, 4H, 2′-H_2), 1.90−1.98 (complex signal, 8H, 2-H_2 and 3- H_2), 2.66 (m, 4H, 1-H_2), 2.99 (m, 4H, 4-H_2), 3.92 (t, $J =$ 7.2 Hz, 4H, 1′-H_2), 7.54 (dd, $J = 9.3$ Hz, $J' = 2.1$ Hz, 2H, 7-H), 7.77 (d, $J \approx 2.1$ Hz, 2H, 5-H), 8.37 (d, $J \approx 9.3$ Hz, 2H, 8-H); ^{13}C NMR (75.4 MHz, CD_3OD) δ 21.8 (CH_2, C3), 22.9 (CH_2, C2), 24.8 (CH_2, C1), 27.6 (CH_2, C3′), 29.4 (CH_2, C4), 30.2 (CH_2) and 31.3 (CH_2) (C2′ and C4′), 49.2 (CH_2, C1′), 113.2 (C, C9a), 115.3 (C, C8a), 119.0 (CH, C5), 126.6 (CH, C7), 128.7 (CH, C8), 139.9 (C, C6), 140.3 (C, C10a), 152.0 (C, C4a), 157.5 (C, C9).

General Procedure for the Preparation of Amides 18−27 from Esters 11 or 12 and Amines 17. A.1. Hydrolysis of Ester 11. A solution of ester **11** (1 mmol) and aqueous 5 N NaOH (1.2 mL, 6 equiv) in MeOH (56 mL) was heated under reflux with magnetic stirring for 16 h. The resulting mixture was cooled to 0 °C (ice−water bath), treated with aqueous 2 N HCl (5.5 mL, 11 equiv), and concentrated in vacuo. The obtained solid residue was extracted with MeOH (18 mL), and the organic extract was evaporated at reduced pressure to give the hydrochloride of the corresponding carboxylic acid, **13**, as a white solid, which was used in the next step without further purification.

A.2. Hydrolysis of Ester 12. A solution of ester **12** (1 mmol) and KOH pellets (240 mg of 85% purity reagent, 3.6 equiv) in MeOH (25 mL) was heated under reflux with magnetic stirring for 24 h. The resulting mixture was cooled to room temperature and evaporated in vacuo. The obtained solid residue was treated with a solution of HCl in Et_2O (20 equiv) with stirring for 30 min, and the suspension was evaporated in vacuo to give the hydrochloride of the corresponding carboxylic acid, **14**, as a white solid, which was used in the next step without further purification.

B. Reaction of Carboxylic Acids 13 or 14 with Amines 17. To a cold solution (0 °C, ice−water bath) of **13** or **14** (crude product arising from 1 mmol of the starting ester **11** or **12**) and anhydrous Et_3N (2.2 mmol) in anhydrous CH_2Cl_2 (50 mL), ethyl chloroformate (1 mmol) was added and the mixture was thoroughly stirred at 0 °C for 30 min. To the resulting solution, a cold solution (0 °C, ice−water bath) of amine **17** (1 mmol) in anhydrous CH_2Cl_2 (50 mL) was added, and the reaction mixture was stirred at room temperature for 64−72 h and treated with 10% aqueous Na_2CO_3 until pH 10 (95 mL). The organic phase was separated, and the aqueous one was extracted with CH_2Cl_2 (3 × 40 mL). The organic phase and combined extracts were washed with water (2 × 80 mL), dried with anhydrous Na_2SO_4, and evaporated at reduced pressure to give a yellow oily residue, which was subjected to column chromatography (35−70 μm silica gel, hexane/AcOEt/Et_3N or heptane/AcOEt/Et_3N mixtures as eluent) to afford the amides **18**−**27** as yellowish oils.

The isolated hybrids **18**−**27** were transformed into the corresponding dihydrochlorides as follows: A solution of the free base (1 mmol) in CH_2Cl_2 (10−60 mL) was filtered through a 0.45 μm PTFE filter and treated with excess of a methanolic solution of HCl (6 mmol). The solution was concentrated in vacuo to dryness, and the solid residue was, in general, recrystallized from MeOH/AcOEt mixtures and dried at 65 °C/15 Torr for 4 days.

6-Chloro-9-{{6-[5-(4-chlorophenyl)-3,4-dihydro-2*H*-pyrano[3,2-*c*]quinoline-9-carboxamido]hexyl}amino}-1,2,3,4-tetrahydroacridine Dihydrochloride (18·2HCl). From crude **13** [173 mg of the crude product obtained from 136 mg (0.37 mmol) of ester **11**] and amine **17c** (126 mg, 0.37 mmol), a brown oily residue (212 mg) was obtained and subjected to column chromatography [35−70 μm silica gel (20 g), hexane/AcOEt/Et_3N mixtures]. On elution with hexane/AcOEt/Et_3N, 20:80:0.05 to 0:100:0.05, hybrid **18** (56 mg, 23% yield) was isolated as a yellowish oil: $R_f = 0.52$ (AcOEt/Et_3N, 10:0.05). **18·2HCl**: mp 194−195 °C (CH_2Cl_2). IR (KBr) ν 3500−2500 (max at 3393, 3253, 3056, 2928, 2856, N−H, $^+$N−H, O−H, and C−H st), 1633 and 1575 (C=O, ar−C−C and ar−C−N st) cm^{-1}; ^{1}H NMR (500 MHz, CD_3OD) δ 1.46−1.56 (complex signal, 4H, 3′-H_2 and 4′-H_2), 1.70 (tt, $J \approx J' \approx 7.0$ Hz, 2H, 5′-H_2), 1.88 (tt, $J = J' = 7.0$ Hz, 2H, 2′-H_2), 1.92−1.99 (complex signal, 4H, 2-H_2 and 3-H_2), 2.16 (tt, $J = J' = 6.0$ Hz, 2H, 3″-H_2), 2.68 (t, $J = 6.0$ Hz, 2H, 1-H_2), 2.85 (t, $J = 6.0$ Hz, 2H, 4″-H_2), 2.98 (t, $J = 6.0$ Hz, 2H, 4-H_2), 3.45 (t, $J = 7.0$ Hz, 2H, 6′-H_2), 3.96 (t, $J = 7.0$ Hz, 2H, 1′-H_2), 4.76 (t, $J \approx 6.0$ Hz, 2H, 2″-H_2), 4.85 (s, NH and $^+$NH), 7.53 (dd, $J = 9.5$ Hz, $J' = 2.0$ Hz, 1H, 7-H), 7.69 [dm, $J = 8.5$ Hz, 2H, 3(5)-H *p*-chlorophenyl], superimposed in part 7.73 [dm, $J = 8.5$ Hz, 2H, 2(6)-H *p*-chlorophenyl], 7.74 (d, $J = 2.0$ Hz, 1H, 5-H), 8.09 (d, $J \approx 9.0$ Hz, 1H, 7″-H), 8.34 (dd, $J = 9.0$ Hz, $J' = 2.0$ Hz, 1H, 8″-H), 8.38 (d, $J = 9.5$ Hz, 1H, 8-H), 8.79 (d, $J = 2.0$ Hz, 1H, 10″-H); ^{13}C NMR (100.6 MHz, CD_3OD) δ 21.72 (CH_2, C3″), 21.74 (CH_2, C3), 22.9 (CH_2, C2), 23.7 (CH_2, C4″), 24.7 (CH_2, C1), 27.2 (CH_2) and 27.5 (CH_2) (C3′and C4′), 29.3 (CH_2, C4), 30.2 (CH_2, C5′), 31.2 (CH_2, C2′), 40.9 (CH_2, C6′), 49.1 (CH_2, C1′), 70.9 (CH_2, C2″), 113.4 (C, C9a), 115.2 (C, C4a″), 115.4 (C, C8a), 119.1 (CH, C5), 120.5 (C, C10a″), 122.9 (CH, C7″), 123.3 (CH, C10″), 126.7 (CH, C7), 128.8 (CH, C8), 130.4 [CH, C3(5) *p*-chlorophenyl], 132.0 [CH, C2(6) *p*-chlorophenyl], 132.7 (CH + C, C8″ and C1 *p*-chlorophenyl), 135.0 (C, C9″), 138.7 (C, C4 *p*-chlorophenyl), 140.0 (C, C6), 140.5 (C, C10a), 142.2 (C, C6a″), 152.1 (C, C4a), 157.8 (C, C9), 158.6 (C, C5″), 166.2 (C, C10b″), 168.0 (C, CONH). HRMS calcd for ($C_{38}H_{38}{}^{35}Cl_2N_4O_2 + H^+$) 653.2450, found 653.2432. Anal. ($C_{38}H_{38}Cl_2N_4O_2 \cdot 2HCl \cdot 2.4H_2O$) C, H, N.

6-Chloro-9-{{8-[3-(3,4-dihydro-5-phenyl-2*H*-pyrano[3,2-*c*]quinolin-9-yl)propanamido]octyl}amino}-1,2,3,4-tetrahydroacridine Dihydrochloride (27·2HCl). From crude **14** [126 mg of the crude product obtained from 122 mg (0.35 mmol) of ester **12**] and amine **17e** (126 mg, 0.35 mmol), a yellow oily residue (198 mg) was obtained and subjected to column chromatography [35−70 μm silica gel (19 g), heptane/AcOEt/Et_3N mixtures]. On elution with heptane/AcOEt/Et_3N, 20:80:0.1, hybrid **27** (91 mg, 39% yield) was isolated as a yellowish oil: $R_f = 0.68$ (AcOEt/MeOH/Et_3N, 90:10:0.1). **27·2HCl**: mp 190−191 °C (MeOH). IR (KBr) ν 3500−2500 (max at 3389, 3245, 3056, 2925, 2853, N−H, $^+$N−H, O−H, and C−H st), 1633 and 1576 (C=O, ar−C−C, and ar−C−N st) cm^{-1}; ^{1}H NMR (500 MHz, CD_3OD) δ 1.20−1.36 (complex signal, 6H, 4′-H_2, 5′-H_2, and 6′-H_2), 1.37−1.45 (complex signal, 4H, 3′-H_2, and 7′-H_2), 1.81 (quint, $J = 7.5$ Hz, 2H, 2′-H_2), 1.91−1.99 (complex signal, 4H, 2-H_2, and 3-H_2), 2.15 (quint, $J \approx 6.0$ Hz, 2H, 3″-H_2), 2.62 (t, $J = 7.5$ Hz, 2H, 9″-CH_2−CH_2-CONH), 2.66 (t, $J = 6.0$ Hz, 2H, 1-H_2), 2.83

(t, J = 6.5 Hz, 2H, 4″-H_2), 2.99 (t, J = 6.0 Hz, 2H, 4-H_2), 3.10 (t, J = 7.5 Hz, 2H, 8′-H_2), 3.18 (t, J = 7.5 Hz, 2H, 9″-CH_2-CH_2−CONH), 3.92 (t, J = 7.5 Hz, 2H, 1′-H_2), 4.76 (t, J = 5.0 Hz, 2H, 2″-H_2), 4.84 (s, NH and $^+$NH), 7.55 (dd, J = 9.5 Hz, J' = 2.0 Hz, 1H, 7-H), 7.65−7.74 [complex signal, 5H, Ar-H phenyl], 7.77 (d, J = 2.0 Hz, 1H, 5-H), 7.94 (dd, J = 9.0 Hz, J' = 1.5 Hz, 1H, 8″-H), 8.00 (d, J = 9.0 Hz, 1H, 7″-H), 8.21 (d, J = 1.5 Hz, 1H, 10″-H), 8.37 (d, $J \approx$ 9.5 Hz, 1H, 8-H); ^{13}C NMR (100.6 MHz, CD_3OD) δ 21.8 (CH_2, C3″), 21.9 (CH_2, C3), 22.9 (CH_2, C2), 23.8 (CH_2, C4″), 24.7 (CH_2, C1′), 27.6 (CH_2, C3′), 27.7 (CH_2, C6′), 29.3 (CH_2, C4), 30.1 (CH_2) and 30.2 (CH_2) (C4′ and C5′), 30.3 (CH_2, C7′), 31.3 (CH_2, C2′), 32.8 (CH_2, 9″-CH$_2$-CH_2-CONH), 38.1 (CH_2, 9″-CH_2-CH$_2$-CONH), 40.3 (CH_2, C8′), 49.2 (CH_2, C1′), 70.6 (CH_2, C2″), 113.3 (C, C9a), 114.2 (C, C4a″), 115.4 (C, C8a), 119.1 (CH, C5), 121.0 (C, C10a″), 122.3 (2 CH, C7″ and C10″), 126.8 (CH, C7), 128.8 (CH, C8), 130.2 (CH) and 132.2 (CH + C) [C1, C2(6), C3(5), and C4 phenyl], 135.9 (CH, C8″), 139.7 (C, C6a″), 140.1 (C, C6), 140.5 (C, C10a), 142.9 (C, C9″), 152.1 (C, C4a), 157.8 (C, C5″), 157.9 (C, C9), 165.1 (C, C10b″), 174.3 (C, CONH). HRMS calcd for ($C_{42}H_{47}{}^{35}ClN_4O_2$ + H^+) 675.3460, found 675.3457. Anal. ($C_{42}H_{47}ClN_4O_2 \cdot 2HCl \cdot 2.25H_2O$) C, H, N.

Biochemical Studies. AChE and BChE Inhibition Assay. AChE inhibitory activity was evaluated spectrophotometrically at 25 °C by the method of Ellman,[64] using AChE from bovine or human erythrocytes and acetylthiocholine iodide (0.53 or 0.13 mM for bAChE and hAChE, respectively) as substrate. The reaction took place in a final volume of 3 mL of 0.1 M phosphate-buffered solution, pH 8.0, containing 0.025 or 0.04 units of bAChE or hAChE, respectively, and 333 μM 5,5′-dithiobis(2-nitrobenzoic) acid (DTNB) solution used to produce the yellow anion of 5-thio-2-nitrobenzoic acid. Inhibition curves were performed in triplicate by incubating at least 12 concentrations of inhibitor for 15 min. One triplicate sample without inhibitor was always present to yield 100% of AChE activity. The reaction was stopped with 100 μL of 1 mM eserine, and the color production was measured at 414 nm. BChE inhibitory activity determinations were carried out similarly, using 0.035 unit of human serum BChE and 0.56 mM butyrylthiocholine, instead of AChE and acetylthiocholine, in a final volume of 1 mL.

Data from concentration−inhibition experiments of the inhibitors were calculated by nonlinear regression analysis, using the GraphPad Prism program package (GraphPad Software; San Diego, CA), which gave estimates of the IC_{50} (concentration of drug producing 50% of enzyme activity inhibition). Results are expressed as the mean ± SEM of at least four experiments performed in triplicate. DTNB, acetylthiocholine, butyrylthiocholine, and enzymes were purchased from Sigma, and eserine was purchased from Fluka.

Kinetic Analysis of AChE Inhibition. To obtain estimates of the mechanism of action of **20**, reciprocal plots of 1/velocity versus 1/[substrate] were constructed at relatively low concentration of substrate (0.56−0.11 mM) by using Ellman's method[64] and human recombinant AChE (Sigma, Milan, Italy). Three concentrations of **20** were selected for this study: 1.25, 1.88, and 3.75 nM. The plots were assessed by a weighted least-squares analysis that assumed the variance of the velocity (v) to be a constant percentage of v for the entire data set. Data analysis was performed with GraphPad Prism 4.03 software (GraphPad Software Inc.).

Slopes of the obtained reciprocal plots were then plotted against **20** concentration in a similar weighted analysis, and K_i was determined as the intercept on the negative x-axis.

AChE-Induced Aβ_{1-40} Aggregation Inhibition Assay. Thioflavin T (Basic Yellow 1), human recombinant AChE lyophilized powder, 1,1,1,3,3,3-hexafluoro-2-propanol (HFIP), were purchased from Sigma Chemicals. Absolute DMSO over molecular sieves was from Fluka. Water was deionized and doubly distilled. Aβ_{1-40}, supplied as trifluoroacetate salt, was purchased from Bachem AG (Bubendorf, Switzerland). Aβ_{1-40} (2 mg mL^{-1}) was dissolved in HFIP and lyophilized. The 1 mM solutions of tested inhibitors were prepared by dissolution in MeOH.

Aliquots of 2 μL Aβ_{1-40} peptide, lyophilized from 2 mg mL^{-1} HFIP solution and dissolved in DMSO, were incubated for 24 h at room temperature in 0.215 M sodium phosphate buffer (pH 8.0) at a final concentration of 230 μM. For co-incubation experiments aliquots (16 μL) of hAChE (final concentration 2.30 μM, Aβ/AChE molar ratio 100:1) and AChE in the presence of 2 μL of the tested inhibitor (final inhibitor concentration 100 μM) in 0.215 M sodium phosphate buffer, pH 8.0, solution were added. Blanks containing Aβ_{1-40} alone, human recombinant AChE alone, and Aβ_{1-40} plus tested inhibitors in 0.215 M sodium phosphate buffer (pH 8.0) were prepared. The final volume of each vial was 20 μL. Each assay was run in duplicate. To quantify amyloid fibril formation, the thioflavin T fluorescence method was then applied.[88] The fluorescence intensities due to β-sheet conformation were monitored for 300 s at λ_{em} = 490 nm (λ_{exc} = 446 nm). The percent inhibition of the AChE-induced aggregation due to the presence of the tested compound was calculated by the following expression: 100 − [(IF_i/IF_o) × 100)] where IF_i and IF_o are the fluorescence intensities obtained for Aβ plus AChE in the presence and in the absence of inhibitor, respectively, minus the fluorescence intensities due to the respective blanks.

Aβ_{1-42} Self-Aggregation Inhibition Assay. As reported in a previously published protocol,[99] HFIP pretreated Aβ_{1-42} samples (Bachem AG, Switzerland) were solubilized with a CH_3CN/Na_2CO_3/NaOH (48.4:48.4:3.2) mixture. Experiments were performed by incubating the peptide in 10 mM phosphate buffer (pH 8.0) containing 10 mM NaCl at 30 °C for 24 h (final Aβ concentration 50 μM) with and without inhibitor (50 μM, Aβ/inhibitor = 1/1). Blanks containing the tested inhibitors were also prepared and tested. To quantify amyloid fibrils formation, the thioflavin T fluorescence method was used.[88] After incubation, samples were diluted to a final volume of 2.0 mL with 50 mM glycine−NaOH buffer (pH 8.5) containing 1.5 μM thioflavin T. A 300 s time scan of fluorescence intensity was carried out (λ_{exc} = 446 nm; λ_{em} = 490 nm, FP-6200 fluorometer, Jasco Europe), and values at plateau were averaged after subtracting the background fluorescence of 1.5 μM thioflavin T solution. The fluorescence intensities were compared, and the percent inhibition due to the presence of the inhibitor was calculated by the following formula 100 − [(IF_i/IF_o) × 100] where IF_i and IF_o are the fluorescence intensities obtained for Aβ_{1-42} in the presence and in the absence of inhibitor, respectively.

β-Secretase (BACE-1) Inhibition Assay. β-Secretase (BACE-1, Sigma) inhibition studies were performed by employing a peptide mimicking APP sequence as substrate (M-2420, Bachem). The following procedure was employed: an amount of 5 μL of test compound (or DMSO) was preincubated with 175 μL of the enzyme (c = 17.2 nM) for 1 h at room temperature. The substrate (3 μM) was then added and left to react for 15 min. The fluorescence signal was read at λ_{em} = 405 nm (λ_{exc} = 320 nm). The fluorescence intensities with and without inhibitor were compared, and the percent inhibition due to the presence of test compounds was calculated. The % inhibition due to the presence of increasing test compound concentration was calculated by the following expression: 100 − [(IF_i/IF_o) × 100], where IF_i and IF_o are the fluorescence intensities obtained for BACE-1 in the presence and in the absence of inhibitor, respectively. Inhibition curve was obtained for **27** by plotting the % inhibition versus the logarithm of inhibitor concentration in the assay sample. The linear regression parameters were determined and the IC_{50} was extrapolated, when possible (GraphPad Prism 4.0, GraphPad Software Inc.).

To demonstrate inhibition of BACE-1 activity, a peptidomimetic inhibitor (β-secretase inhibitor IV, Calbiochem) was serially diluted into the reactions' wells (IC_{50} = 0.013 μM).

Molecular Modeling. Docking was performed with the program rDock, which is an extension of the program RiboDock,[100] using an empirical scoring function calibrated on the basis of protein−ligand complexes.[101] The reliability of rDock was assessed by docking a set of known dual binding site AChEIs taking advantage of the X-ray crystallographic structures of their complexes with AChE (PDB entries 1Q83, 1Q84, 1ODC, 1ZGB, 1ZGC, 2CKM, and 2CMF), which was also chosen to identify three different orientations of the indole ring of Trp286 in the peripheral binding site in hAChE (see Molecular Modeling Studies and also Tables S2 and S3 in Supporting Information).

The docking of compounds **20**, **25**, and **27** in hAChE was then explored using the three structural models of the target hAChE (named A, B, and C). Structural water molecules that mediate relevant interactions between the tacrine moiety and the enzyme were retained in the target models. The docking volume was defined as the space within 10 Å of the ligands spanning both catalytic and peripheral binding sites. The ligands were considered in their monocationic form on the basis of the pK_a estimated using ACD software.[102] The structure of the ligands was initially energy minimized at the AM1[103] level using Gaussian 03.[104] Suitable restraints were introduced to position the tacrine moiety of the hybrids in the catalytic site, as inspection of the X-ray crystallographic structures of several tacrine-based dual binding site AChEIs reveals that the tacrine unit shares a common binding mode, which in turn mimics the pose found for AChE complexes with tacrine[7] and huprine X[69] (see text). This allowed us to focus the sampling effort on the orientation of the pyrano[3,2-*c*]quinoline unit of the hybrids at the peripheral binding site and the linker along the gorge. Each compound was subjected to 100 docking runs, and the output docking modes were analyzed by visual inspection in conjunction with the docking scores.

The ligand−protein poses were reranked using the MM−PBSA approach (Table S4, Supporting Information). An energy minimization of the complexes was first carried out in order to reduce steric clashes that might arise from docking calculations. All minimizations and MM-PBSA calculations were performed with the parmm99 force field of the Amber-9 package.[105] The relative binding affinities of the best poses of the ligands were determined by using eq 1.

$$\Delta G_{\text{binding}} = \Delta G_{\text{MM}} + \Delta G^{\text{sol}}_{\text{ele}} + \Delta G^{\text{sol}}_{\text{nonpolar}} - T\Delta S \qquad (1)$$

The partial atomic charges for the compounds were derived using the RESP protocol[106] by fitting to the molecular electrostatic potential calculated at the HF/6-31G* level with Gaussian 03. The internal conformational energy (ΔG_{MM}) was determined using the standard formalism and parameters implemented in AMBER. The electrostatic contribution ($\Delta G^{\text{sol}}_{\text{ele}}$) was computed using a dielectric constant of 78.4 for the aqueous environment, while values of 2 and 4 were considered for the ligand−enzyme complex. The electrostatic potentials were calculated using a grid spacing of 0.25 Å. The interior of the solutes was defined as the volume inaccessible to a solvent probe sphere of radius 1.4 Å. The nonpolar contribution ($\Delta G^{\text{sol}}_{\text{nonpolar}}$) was calculated using a linear dependence with the solvent-accessible surface.[107] Finally, entropy changes upon complexation were assumed to cancel out in the comparison of the binding affinities of **20** and **25**, as the number of rotatable bonds is the same in both compounds. However, since the spacer of **27** is larger by two methylene units, its binding affinity was corrected for the entropic penalty associated with the freezing of the two extra internal degrees of freedom using an empirical correction of 0.6 kcal/mol per rotatable bond.[108,109]

Finally, molecular dynamics simulations were run to further check the stability of the proposed binding mode for compounds **20** and **25**. Simulations were performed using the same protocol adopted in our previous studies,[31,109] which also enabled us to predict the binding mode of huprines to AChE.[110] Briefly, the enzyme was immersed in a pre-equilibrated box of TIP3P[111] water molecules. The final systems contained the protein−ligand complex and around 16 000 water molecules (about 57 000 atoms). After thermatilization at 298 K, a series of 10 ns trajectories were sampled for the different compounds in the receptor−ligand complex. The system was simulated in the NPT ensemble using periodic boundary conditions and Ewald sums for treating long-range electrostatic interactions (with the default Amber-9 parameters). All simulations were performed with the parmm99 force field of the Amber-9 package. The structural analysis was performed using in-house software and standard codes (PTRAJ module) of Amber-9.

In Vitro BBB Permeation Assay. Prediction of the brain penetration was evaluated using a parallel artificial membrane permeation assay (PAMPA) in a similar manner as described previously.[39,52,95−98] Commercial drugs, phosphate buffered saline solution at pH 7.4 (PBS), and dodecane were purchased from Sigma, Aldrich, Acros, and Fluka. Millex filter units (PVDF membrane, diameter 25 mm, pore size 0.45 μm) were acquired from Millipore. The porcine brain lipid (PBL) was obtained from Avanti Polar Lipids. The donor microplate was a 96-well filter plate (PVDF membrane, pore size 0.45 μm), and the acceptor microplate was an indented 96-well plate, both from Millipore. The acceptor 96-well microplate was filled with 180 μL of PBS/EtOH (80:20 or 70:30), and the filter surface of the donor microplate was impregnated with 4 μL of PBL in dodecane (20 mg mL^{-1}). Compounds were dissolved in PBS/EtOH (80:20 or 70:30) at 1 mg mL^{-1}, filtered through a Millex filter, and then added to the donor wells (180 μL). The donor filter plate was carefully put on the acceptor plate to form a sandwich, which was left undisturbed for 120 min at 25 °C. After incubation, the donor plate was carefully removed and the concentration of compounds in the acceptor wells was determined by UV spectroscopy. Every sample was analyzed at five wavelengths, in four wells, and at least in three independent runs, and the results are given as the mean ± standard deviation. In each experiment, 15 quality control standards of known BBB permeability were included to validate the analysis set.

Acknowledgment. Financial support from the Ministerio de Ciencia y Tecnología (MCT) and FEDER (Grants CTQ2008-03768/PPQ, BQU2006-03794, SAF2008-05595, SAF2006-04339, SAF2006-01249), Generalitat de Catalunya (Grants 2005-SGR00180, 2005-SGR00662), MIUR (Grant PRIN 2007) (Rome, Italy), and EU's 7FP funding (BISNES, Grants NMP-2007-1.1-1 and GA n. 214538) and fellowships for C.G. (IBUB) and Ó.H. (MCT) are acknowledged.

Supporting Information Available: Experimental procedures, spectral and analytical data of synthesized compounds (except for **9**−**14**, **17c**,**e**, and **28c**,**e**, **18**, and **27**, herein described); solution stability study with **23**; table with pK_a values of selected compounds; tables and figures with additional data on docking and molecular dynamics; PAMPA-BBB studies. This material is available free of charge via the Internet at http://pubs.acs.org.

References

(1) Inestrosa, N. C.; Alvarez, A.; Pérez, C. A.; Moreno, R. D.; Vicente, M.; Linker, C.; Casanueva, O. I.; Soto, C.; Garrido, J. Acetylcholinesterase Accelerates Assembly of Amyloid-*β*-peptides into Alzheimer's Fibrils: Possible Role of the Peripheral Site of the Enzyme. *Neuron* **1996**, *16*, 881–891.
(2) Inestrosa, N. C.; Dinamarca, M. C.; Alvarez, A. Amyloid−Cholinesterase Interactions. Implications for Alzheimer's Disease. *FEBS J.* **2008**, *275*, 625–632.
(3) Rees, T.; Hammond, P. I.; Soreq, H.; Younkin, S.; Brimijoin, S. Acetylcholinesterase Promotes Beta-Amyloid Plaques in Cerebral Cortex. *Neurobiol. Aging* **2003**, *24*, 777–787.

(4) Rees, T. M.; Berson, A.; Sklan, E. H.; Younkin, L.; Younkin, S.; Brimijoin, S.; Soreq, H. Memory Deficits Correlating with Acetylcholinesterase Splice Shift and Amyloid Burden in Doubly Transgenic Mice. *Curr. Alzheimer Res.* **2005**, *2*, 291–300.
(5) De Ferrari, G. V.; Canales, M. A.; Shin, I.; Weiner, L. M.; Silman, I.; Inestrosa, N. C. A Structural Motif of Acetylcholinesterase That Promotes Amyloid Beta-Peptide Fibril Formation. *Biochemistry* **2001**, *40*, 10447–10457.
(6) Johnson, G.; Moore, S. W. The Peripheral Anionic Site of Acetylcholinesterase: Structure, Functions and Potential Role in Rational Drug Design. *Curr. Pharm. Des.* **2006**, *12*, 217–225.
(7) Harel, M.; Schalk, I.; Ehret-Sabatier, L.; Bouet, F.; Goeldner, M.; Hirth, C.; Axelsen, P. H.; Silman, I.; Sussman, J. L. Quaternary Ligand Binding to Aromatic Residues in the Active-Site Gorge of Acetylcholinesterase. *Proc. Natl. Acad. Sci. U.S.A.* **1993**, *90*, 9031–9035.
(8) Castro, A.; Martinez, A. Peripheral and Dual Binding Site Acetylcholinesterase Inhibitors: Implications in Treatment of Alzheimer's Disease. *Mini-Rev. Med. Chem.* **2001**, *1*, 267–272.
(9) Du, D.-M.; Carlier, P. R. Development of Bivalent Acetylcholinesterase Inhibitors as Potential Therapeutic Drugs for Alzheimer's Disease. *Curr. Pharm. Des.* **2004**, *10*, 3141–3156.
(10) Recanatini, M.; Valenti, P. Acetylcholinesterase Inhibitors as a Starting Point towards Improved Alzheimer's Disease Therapeutics. *Curr. Pharm. Des.* **2004**, *10*, 3157–3166.
(11) Muñoz-Torrero, D.; Camps, P. Dimeric and Hybrid Anti-Alzheimer Drug Candidates. *Curr. Med. Chem.* **2006**, *13*, 763–771.
(12) Castro, A.; Martinez, A. Targeting Beta-Amyloid Pathogenesis through Acetylcholinesterase Inhibitors. *Curr. Pharm. Des.* **2006**, *12*, 4377–4387.
(13) Li, W. M.; Kan, K. K. W.; Carlier, P. R.; Pang, Y. P.; Han, Y. F. East Meets West in the Search for Alzheimer's Therapeutics—Novel Dimeric Inhibitors from Tacrine and Huperzine A. *Curr. Alzheimer Res.* **2007**, *4*, 386–396.
(14) Holzgrabe, U.; Kapková, P.; Alptüzün, V.; Scheiber, J.; Kugelmann, E. Targeting Acetylcholinesterase To Treat Neurodegeneration. *Expert Opin. Ther. Targets* **2007**, *11*, 161–179.
(15) Musial, A.; Bajda, M.; Malawska, B. Recent Developments in Cholinesterases Inhibitors for Alzheimer's Disease Treatment. *Curr. Med. Chem.* **2007**, *14*, 2654–2679.
(16) Haviv, H.; Wong, D. M.; Silman, I.; Sussman, J. L. Bivalent Ligands Derived from Huperzine A as Acetylcholinesterase Inhibitors. *Curr. Top. Med. Chem.* **2007**, *7*, 375–387.
(17) Cavalli, A.; Bolognesi, M. L.; Minarini, A.; Rosini, M.; Tumiatti, V.; Recanatini, M.; Melchiorre, C. Multi-Target-Directed Ligands To Combat Neurodegenerative Diseases. *J. Med. Chem.* **2008**, *51*, 347–372.
(18) Muñoz-Torrero, D. Acetylcholinesterase Inhibitors as Disease-Modifying Therapies for Alzheimer's Disease. *Curr. Med. Chem.* **2008**, *15*, 2433–2455.
(19) Piazzi, L.; Rampa, A.; Bisi, A.; Gobbi, S.; Belluti, F.; Cavalli, A.; Bartolini, M.; Andrisano, V.; Valenti, P.; Recanatini, M. 3-(4-{[Benzyl(methyl)amino]methyl}phenyl)-6,7-dimethoxy-2*H*-2-chromenone (AP2238) Inhibits Both Acetylcholinesterase and Acetylcholinesterase-Induced *β*-Amyloid Aggregation: A Dual Function Lead for Alzheimer's Disease Therapy. *J. Med. Chem.* **2003**, *46*, 2279–2282.
(20) Tumiatti, V.; Andrisano, V.; Banzi, R.; Bartolini, M.; Minarini, A.; Rosini, M.; Melchiorre, C. Structure−Activity Relationships of Acetylcholinesterase Noncovalent Inhibitors Based on a Polyamine Backbone. 3. Effect of Replacing the Inner Polymethylene Chain with Cyclic Amines. *J. Med. Chem.* **2004**, *47*, 6490–6498.
(21) Bolognesi, M. L.; Andrisano, V.; Bartolini, M.; Banzi, R.; Melchiorre, C. Propidium-Based Polyamine Ligands as Potent Inhibitors of Acetylcholinesterase and Acetylcholinesterase-Induced Amyloid-*β* Aggregation. *J. Med. Chem.* **2005**, *48*, 24–27.
(22) Rosini, M.; Andrisano, V.; Bartolini, M.; Bolognesi, M. L.; Hrelia, P.; Minarini, A.; Tarozzi, A.; Melchiorre, C. Rational Approach To Discover Multipotent Anti-Alzheimer Drugs. *J. Med. Chem.* **2005**, *48*, 360–363.
(23) Muñoz-Ruiz, P.; Rubio, L.; García-Palomero, E.; Dorronsoro, I.; del Monte-Millán, M.; Valenzuela, R.; Usán, P.; de Austria, C.; Bartolini, M.; Andrisano, V.; Bidon-Chanal, A.; Orozco, M.; Luque, F. J.; Medina, M.; Martínez, A. Design, Synthesis, and Biological Evaluation of Dual Binding Site Acetylcholinesterase Inhibitors: New Disease-Modifying Agents for Alzheimer's Disease. *J. Med. Chem.* **2005**, *48*, 7223–7233.
(24) Belluti, F.; Rampa, A.; Piazzi, L.; Bisi, A.; Gobbi, S.; Bartolini, M.; Andrisano, V.; Cavalli, A.; Recanatini, M.; Valenti, P. Cholinesterase Inhibitors: Xanthostigmine Derivatives Blocking the Acetylcholinesterase-Induced *β*-Amyloid Aggregation. *J. Med. Chem.* **2005**, *48*, 4444–4456.
(25) Piazzi, L.; Cavalli, A.; Belluti, F.; Bisi, A.; Gobbi, S.; Rizzo, S.; Bartolini, M.; Andrisano, V.; Recanatini, M.; Rampa, A. Extensive SAR and Computational Studies of 3-{4-[(Benzylmethylamino)methyl]phenyl}-6,7-dimethoxy-2*H*-2-chromenone (AP2238) Derivatives. *J. Med. Chem.* **2007**, *50*, 4250–4254.
(26) Cavalli, A.; Bolognesi, M. L.; Capsoni, S.; Andrisano, V.; Bartolini, M.; Margotti, E.; Cattaneo, A.; Recanatini, M.; Melchiorre, C. A Small Molecule Targeting the Multifactorial Nature of Alzheimer's Disease. *Angew. Chem., Int. Ed.* **2007**, *46*, 3689–3692.
(27) Bolognesi, M. L.; Banzi, R.; Bartolini, M.; Cavalli, A.; Tarozzi, A.; Andrisano, V.; Minarini, A.; Rosini, M.; Tumiatti, V.; Bergamini, C.; Fato, R.; Lenaz, G.; Hrelia, P.; Cattaneo, A.; Recanatini, M.; Melchiorre, C. Novel Class of Quinone-Bearing Polyamines as Multi-Target-Directed Ligands To Combat Alzheimer's Disease. *J. Med. Chem.* **2007**, *50*, 4882–4897.
(28) Bolognesi, M. L.; Cavalli, A.; Valgimigli, L.; Bartolini, M.; Rosini, M.; Andrisano, V.; Recanatini, M.; Melchiorre, C. Multi-Target-Directed Drug Design Strategy: From a Dual Binding Site Acetylcholinesterase Inhibitor to a Trifunctional Compound against Alzheimer's Disease. *J. Med. Chem.* **2007**, *50*, 6446–6449.
(29) Kwon, Y. E.; Park, J. Y.; No, K. T.; Shin, J. H.; Lee, S. K.; Eun, J. S.; Yang, J. H.; Shin, T. Y.; Kim, D. K.; Chae, B. S.; Leem, J.-Y.; Kim, K. H. Synthesis, in Vitro Assay, and Molecular Modeling of New Piperidine Derivatives Having Dual Inhibitory Potency against Acetylcholinesterase and Aβ_{1-42} Aggregation for Alzheimer's Disease Therapeutics. *Bioorg. Med. Chem.* **2007**, *15*, 6596–6607.
(30) Xie, Q.; Wang, H.; Xia, Z.; Lu, M.; Zhang, W.; Wang, X.; Fu, W.; Tang, Y.; Sheng, W.; Li, W.; Zhou, W.; Zhu, X.; Qiu, Z.; Chen, H. Bis-(−)-nor-meptazinols as Novel Nanomolar Cholinesterase Inhibitors with High Inhibitory Potency on Amyloid-*β* Aggregation. *J. Med. Chem.* **2008**, *51*, 2027–2036.
(31) Camps, P.; Formosa, X.; Galdeano, C.; Gómez, T.; Muñoz-Torrero, D.; Scarpellini, M.; Viayna, E.; Badia, A.; Clos, M. V.; Camins, A.; Pallàs, M.; Bartolini, M.; Mancini, F.; Andrisano, V.; Estelrich, J.; Lizondo, M.; Bidon-Chanal, A.; Luque, F. J. Novel Donepezil-Based Inhibitors of Acetyl- and Butyrylcholinesterase and Acetylcholinesterase-Induced *β*-Amyloid Aggregation. *J. Med. Chem.* **2008**, *51*, 3588–3598.
(32) Rosini, M.; Simoni, E.; Bartolini, M.; Cavalli, A.; Ceccarini, L.; Pascu, N.; McClymont, D. W.; Tarozzi, A.; Bolognesi, M. L.; Minarini, A.; Tumiatti, V.; Andrisano, V.; Mellor, I. R.; Melchiorre, C. Inhibition of Acetylcholinesterase, *β*-Amyloid Aggregation, and NMDA Receptors in Alzheimer's Disease: A Promising Direction for the Multi-Target-Directed Ligands Gold Rush. *J. Med. Chem.* **2008**, *51*, 4381–4384.
(33) Tumiatti, V.; Milelli, A.; Minarini, A.; Rosini, M.; Bolognesi, M. L.; Micco, M.; Andrisano, V.; Bartolini, M.; Mancini, F.; Recanatini, M.; Cavalli, A.; Melchiorre, C. Structure−Activity Relationships of Acetylcholinesterase Noncovalent Inhibitors Based on a Polyamine Backbone. 4. Further Investigation on the Inner Spacer. *J. Med. Chem.* **2008**, *51*, 7308–7312.
(34) Bolognesi, M. L.; Bartolini, M.; Rosini, M.; Andrisano, V.; Melchiorre, C. Structure−Activity Relationships of Memoquin: Influence of the Chain Chirality in the Multi-Target Mechanism of Action. *Bioorg. Med. Chem. Lett.* **2009**, *19*, 4312–4315.
(35) García-Palomero, E.; Muñoz, P.; Usan, P.; Garcia, P.; De Austria, C.; Valenzuela, R.; Rubio, L.; Medina, M.; Martínez, A. Potent *β*-Amyloid Modulators. *Neurodegener. Dis.* **2008**, *5*, 153–156.
(36) Pang, Y.-P.; Quiram, P.; Jelacic, T.; Hong, F.; Brimijoin, S. Highly Potent, Selective, and Low Cost Bis-tetrahydroaminacrine Inhibitors of Acetylcholinesterase. *J. Biol. Chem.* **1996**, *271*, 23646–23649.
(37) Zhang, L.; Yu, H.; Li, W. M.; Cheung, M. C.; Pang, Y. P.; Gu, Z. M.; Chan, K.; Wang, Y. T.; Zuo, Z.; Han, Y. F. Preclinical Characterization of Intestinal Absorption and Metabolism of Promising Anti-Alzheimer's Dimer Bis(7)-tacrine. *Int. J. Pharm.* **2008**, *357*, 85–94.
(38) http://www.noscira.com.
(39) Rodríguez-Franco, M. I.; Fernández-Bachiller, M. I.; Pérez, C.; Hernández-Ledesma, B.; Bartolomé, B. Novel Tacrine−Melatonin Hybrids as Dual-Acting Drugs for Alzheimer Disease, with Improved Acetylcholinesterase Inhibitory and Antioxidant Properties. *J. Med. Chem.* **2006**, *49*, 459–462.
(40) Gemma, S.; Gabellieri, E.; Huleatt, P.; Fattorusso, C.; Borriello, M.; Catalanotti, B.; Butini, S.; De Angelis, M.; Novellino, E.; Nacci, V.; Belinskaya, T.; Saxena, A.; Campiani, G. Discovery of Huperzine A−Tacrine Hybrids as Potent Inhibitors of Human Cholinesterases Targeting Their Midgorge Recognition Sites. *J. Med. Chem.* **2006**, *49*, 3421–3425.

(41) Decker, M. Homobivalent Quinazolinimines as Novel Nanomolar Inhibitors of Cholinesterases with Dirigible Selectivity toward Butyrylcholinesterase. *J. Med. Chem.* **2006**, *49*, 5411–5413.
(42) Elsinghorst, P. W.; González Tanarro, C. M.; Gütschow, M. Novel Heterobivalent Tacrine Derivatives as Cholinesterase Inhibitors with Notable Selectivity toward Butyrylcholinesterase. *J. Med. Chem.* **2006**, *49*, 7540–7544.
(43) Sauvaître, T.; Barlier, M.; Herlem, D.; Gresh, N.; Chiaroni, A.; Guenard, D.; Guillou, C. New Potent Acetylcholinesterase Inhibitors in the Tetracyclic Triterpene Series. *J. Med. Chem.* **2007**, *50*, 5311–5323.
(44) Elsinghorst, P. W.; Cieslik, J. S.; Mohr, K.; Tränkle, C.; Gütschow, M. First Gallamine−Tacrine Hybrid: Design and Characterization at Cholinesterases and the M_2 Muscarinic Receptor. *J. Med. Chem.* **2007**, *50*, 5685–5695.
(45) He, X.-C.; Feng, S.; Wang, Z.-F.; Shi, Y.; Zheng, S.; Xia, Y.; Jiang, H.; Tang, X.-C.; Bai, D. Study on Dual-Site Inhibitors of Acetylcholinesterase: Highly Potent Derivatives of Bis- and Bifunctional Huperzine B. *Bioorg. Med. Chem.* **2007**, *15*, 1394–1408.
(46) Butini, S.; Campiani, G.; Borriello, M.; Gemma, S.; Panico, A.; Persico, M.; Catalanotti, B.; Ros, S.; Brindisi, M.; Agnusdei, M.; Fiorini, I.; Nacci, V.; Novellino, E.; Belinskaya, T.; Saxena, A.; Fattorusso, C. Exploiting Protein Fluctuations at the Active-Site Gorge of Human Cholinesterases: Further Optimization of the Design Strategy To Develop Extremely Potent Inhibitors. *J. Med. Chem.* **2008**, *51*, 3154–3170.
(47) Pan, L.; Tan, J.-H.; Hou, J.-Q.; Huang, S.-L.; Gu, L.-Q.; Huang, Z.-S. Design, Synthesis and Evaluation of Isaindigotone Derivatives as Acetylcholinesterase and Butyrylcholinesterase Inhibitors. *Bioorg. Med. Chem. Lett.* **2008**, *18*, 3790–3793.
(48) Butini, S.; Guarino, E.; Campiani, G.; Brindisi, M.; Coccone, S. S.; Fiorini, I.; Novellino, E.; Belinskaya, T.; Saxena, A.; Gemma, S. Tacrine Based Human Cholinesterase Inhibitors: Synthesis of Peptidic-Tethered Derivatives and Their Effect on Potency and Selectivity. *Bioorg. Med. Chem. Lett.* **2008**, *18*, 5213–5216.
(49) Bembenek, S. D.; Keith, J. M.; Letavic, M. A.; Apodaca, R.; Barbier, A. J.; Dvorak, L.; Aluisio, L.; Miller, K. L.; Lovenberg, T. W.; Carruthers, N. I. Lead Identification of Acetylcholinesterase Inhibitors−Histamine H_3 Receptor Antagonists from Molecular Modeling. *Bioorg. Med. Chem.* **2008**, *16*, 2968–2973.
(50) Leonetti, F.; Catto, M.; Nicolotti, O.; Pisani, L.; Cappa, A.; Stefanachi, A.; Carotti, A. Homo- and Hetero-Bivalent Edrophonium-Like Ammonium Salts as Highly Potent, Dual Binding Site AChE Inhibitors. *Bioorg. Med. Chem.* **2008**, *16*, 7450–7456.
(51) Shen, Y.; Sheng, R.; Zhang, J.; He, Q.; Yang, B.; Hu, Y. 2-Phenoxy-indan-1-one Derivatives as Acetylcholinesterase Inhibitors: A Study on the Importance of Modifications at the Side Chain on the Activity. *Bioorg. Med. Chem.* **2008**, *16*, 7646–7653.
(52) Fernández-Bachiller, M. I.; Pérez, C.; Campillo, N. E.; Páez, J. A.; González-Muñoz, G. C.; Usán, P.; García-Palomero, E.; López, M. G.; Villarroya, M.; García, A. G.; Martínez, A.; Rodríguez-Franco, M. I. Tacrine−Melatonin Hybrids as Multifunctional Agents for Alzheimer's Disease, with Cholinergic, Antioxidant, and Neuroprotective Properties. *ChemMedChem* **2009**, *4*, 828–841.
(53) Bourne, Y.; Taylor, P.; Radić, Z.; Marchot, P. Structural Insights into Ligand Interactions at the Acetylcholinesterase Peripheral Anionic Site. *EMBO J.* **2003**, *22*, 1–12.
(54) Cavalli, A.; Bottegoni, G.; Raco, C.; De Vivo, M.; Recanatini, M. A Computational Study of the Binding of Propidium to the Peripheral Anionic Site of Human Acetylcholinesterase. *J. Med. Chem.* **2004**, *47*, 3991–3999.
(55) Jiménez, O.; de la Rosa, G.; Lavilla, R. Straightforward Access to a Structurally Diverse Set of Oxacyclic Scaffolds through a Four-Component Reaction. *Angew. Chem., Int. Ed.* **2005**, *44*, 6521–6525.
(56) Hu, M.-K.; Wu, L.-J.; Hsiao, G.; Yen, M.-H. Homodimeric Tacrine Congeners as Acetylcholinesterase Inhibitors. *J. Med. Chem.* **2002**, *45*, 2277–2282.
(57) Alonso, D.; Dorronsoro, I.; Rubio, L.; Muñoz, P.; García-Palomero, E.; Del Monte, M.; Bidon-Chanal, A.; Orozco, M.; Luque, F. J.; Castro, A.; Medina, M.; Martínez, A. Donepezil−Tacrine Hybrid Related Derivatives as New Dual Binding Site Inhibitors of AChE. *Bioorg. Med. Chem.* **2005**, *13*, 6588–6597.
(58) Povarov, L. S. **α,β**-Unsaturated Ethers and Their Analogues in Reactions of Diene Synthesis. *Russ. Chem. Rev.* **1967**, *36*, 656–670.
(59) Jakobsen, C. M.; Denmeade, S. R.; Isaacs, J. T.; Gady, A.; Olsen, C. E.; Christensen, S. B. Design, Synthesis, and Pharmacological Evaluation of Thapsigargin Analogues for Targeting Apoptosis to Prostatic Cancer Cells. *J. Med. Chem.* **2001**, *44*, 4696–4703.
(60) Carlier, P. R.; Han, Y. F.; Chow, E. S.-H.; Li, C. P.-L.; Wang, H.; Lieu, T. X.; Wong, H. S.; Pang, Y.-P. Evaluation of Short-Tether Bis-THA AChE Inhibitors. A Further Test of the Dual Binding Site Hypothesis. *Bioorg. Med. Chem.* **1999**, *7*, 351–357.
(61) Carlier, P. R.; Chow, E. S.-H.; Han, Y.; Liu, J.; El Yazal, J.; Pang, Y.-P. Heterodimeric Tacrine-Based Acetylcholinesterase Inhibitors: Investigating Ligand−Peripheral Site Interactions. *J. Med. Chem.* **1999**, *42*, 4225–4231.
(62) Hu, M. -K.; Lu, C.-F. A Facile Synthesis of Bis-Tacrine Isosteres. *Tetrahedron Lett.* **2000**, *41*, 1815–1818.
(63) Hu, M.-K.; Shaw, J. Tacrine Derivatives for Treating Alzheimer's Disease. WO 01/17529 A1, 2001.
(64) Ellman, G. L.; Courtney, K. D.; Andres, B., Jr.; Featherstone, R. M. A New and Rapid Colorimetric Determination of Acetylcholinesterase Activity. *Biochem. Pharmacol.* **1961**, *7*, 88–95.
(65) Savini, L.; Gaeta, A.; Fattorusso, C.; Catalanotti, B.; Campiani, G.; Chiasserini, L.; Pellerano, C.; Novellino, E.; McKissic, D.; Saxena, A. Specific Targeting of Acetylcholinesterase and Butyrylcholinesterase Recognition Sites. Rational Design of Novel, Selective, and Highly Potent Cholinesterase Inhibitors. *J. Med. Chem.* **2003**, *46*, 1–4.
(66) Savini, L.; Campiani, G.; Gaeta, A.; Pellerano, C.; Fattorusso, C.; Chiasserini, L.; Fedorko, J. M.; Saxena, A. Novel and Potent Tacrine-Related Hetero- and Homobivalent Ligands for Acetylcholinesterase and Butyrylcholinesterase. *Bioorg. Med. Chem. Lett.* **2001**, *11*, 1779–1782.
(67) Muñoz-Muriedas, J.; López, J. M.; Orozco, M.; Luque, F. J. Molecular Modelling Approaches to the Design of Acetylcholinesterase Inhibitors: New Challenges for the Treatment of Alzheimer's Disease. *Curr. Pharm. Des.* **2004**, *10*, 3131–3140.
(68) Silman, I.; Sussman, J. L. Acetylcholinesterase: "Classical" and "Non-Classical" Functions and Pharmacology. *Curr. Opin. Pharmacol.* **2005**, *5*, 293–302.
(69) Dvir, H.; Wong, D. M.; Harel, M.; Barril, X.; Orozco, M.; Luque, F. J.; Muñoz-Torrero, D.; Camps, P.; Rosenberry, T. L.; Silman, I.; Sussman, J. L. 3D Structure of *Torpedo californica* Acetylcholinesterase Complexed with Huprine X at 2.1 Å Resolution: Kinetic and Molecular Dynamics Correlates. *Biochemistry* **2002**, *41*, 2970–2981.
(70) Rydberg, E. H.; Brumshtein, B.; Greenblatt, H. M.; Wong, D. M.; Shaya, D.; Williams, L. D.; Carlier, P. R.; Pang, Y.-P.; Silman, I.; Sussman, J. L. Complexes of Alkylene-Linked Tacrine Dimers with *Torpedo californica* Acetylcholinesterase: Binding of Bis(5)-Tacrine Produces a Dramatic Rearrangement in the Active-Site Gorge. *J. Med. Chem.* **2006**, *49*, 5491–5500.
(71) Colletier, J. P.; Sanson, B.; Nachon, F.; Gabellieri, E.; Fattorusso, C.; Campiani, G.; Weik, M. Conformational Flexibility in the Peripheral Site of *Torpedo californica* Acetylcholinesterase Revealed by the Complex Structure with a Bifunctional Inhibitor. *J. Am. Chem. Soc.* **2006**, *128*, 4526–4527.
(72) Haviv, H.; Wong, D. M.; Greenblatt, H. M.; Carlier, P. R.; Pang, Y.-P.; Silman, I.; Sussman, J. L. Crystal Packing Mediates Enantioselective Ligand Recognition at the Peripheral Site of Acetylcholinesterase. *J. Am. Chem. Soc.* **2005**, *127*, 11029–11036.
(73) Bourne, Y.; Kolb, H. C.; Radic, Z; Sharpless, K. B.; Taylor, P.; Marchot, P. Freeze-Frame Inhibitor Captures Acetylcholinesterase in a Unique Conformation. *Proc. Natl. Acad. Sci. U.S.A.* **2004**, *101*, 1449–1454.
(74) Senapati, S.; Bui, J. M.; McCammon, J. A. Induced Fit in Mouse Acetylcholinesterase upon Binding a Femtomolar Inhibitor: A Molecular Dynamics Study. *J. Med. Chem.* **2005**, *48*, 8155–8162.
(75) Sussman, J. L.; Harel, M.; Frolow, F.; Oefner, C.; Goldman, A.; Toker, L.; Silman, I. Atomic Structure of Acetylcholinesterase from *Torpedo californica*: A Prototypic Acetylcholine-Binding Protein. *Science* **1991**, *253*, 872–879.
(76) Raves, M. L.; Harel, M.; Pang, Y.-P.; Silman, I.; Kozikowski, A. P.; Sussman, J. L. Structure of Acetylcholinesterase Complexed with the Nootropic Alkaloid, (−)-Huperzine A. *Nat. Struct. Biol.* **1997**, *4*, 57–63.
(77) Kryger, G.; Silman, I.; Sussman, J. L. Structure of Acetylcholinesterase Complexed with E2020 (Aricept): Implications for the Design of New Anti-Alzheimer Drugs. *Structure* **1999**, *7*, 297–307.
(78) Kryger, G.; Harel, M.; Giles, K.; Toker, L.; Velan, B.; Lazar, A.; Kronman, C.; Barak, D.; Ariel, N.; Shafferman, A.; Silman, I.; Sussman, J. L. Structures of Recombinant Native and E202Q Mutant Human Acetylcholinesterase Complexed with the Snake-Venom Toxin Fasciculin-II. *Acta Crystallogr., Sect. D: Biol. Crystallogr.* **2000**, *56*, 1385–1394.
(79) Lyne, P. D.; Lamb, M.; Saeh, J. C. Accurate Prediction of the Relative Potencies of Members of a Series of Kinase Inhibitors Using Molecular Docking and MM-GBSA Scoring. *J. Med. Chem.* **2006**, *49*, 4805–4808.
(80) Weis, A.; Katebzadeh, K.; Soderhjelm, P.; Nilsson, I.; Ryde, U. Ligand Affinities Predicted with the MM/PBSA Method: Dependence

on the Simulation Method and the Force Field. *J. Med. Chem.* **2006**, *49*, 6596–6606.
(81) Stoica, I.; Sadiq, S. K.; Coveney, P. V. Rapid and Accurate Prediction of Binding Free Energies for Saquinavir-Bound HIV-1 Proteases. *J. Am. Chem. Soc.* **2008**, *130*, 2639–2648.
(82) Barril, X.; Gelpí, J. L.; López, J. M.; Orozco, M.; Luque, F. J. How Accurate Can Molecular Dynamics/Linear Response and Poisson−Boltzmann/Solvent Accessible Surface Calculations Be for Predicting Relative Binding Affinities? Acetylcholinesterase Huprine Inhibitors as a Test Case. *Theor. Chem. Acc.* **2001**, *106*, 2–9.
(83) Giacobini, E. Cholinesterase Inhibitors: New Roles and Therapeutic Alternatives. *Pharmacol. Res.* **2004**, *50*, 433–440.
(84) Lane, R. M.; Potkin, S. G.; Enz, A. Targeting Acetylcholinesterase and Butyrylcholinesterase in Dementia. *Int. J. Neuropsychopharmacol.* **2005**, *9*, 1–24.
(85) Gregor, V. E.; Emmerling, M. R.; Lee, C.; Moore, C. J. The Synthesis and in Vitro Acetylcholinesterase and Butyrylcholinesterase Inhibitory Activity of Tacrine (Cognex) Derivatives. *Bioorg. Med. Chem. Lett.* **1992**, *2*, 861–864.
(86) Wlodek, S. T.; Antosiewicz, J.; McCammon, J. A.; Straatsma, T. P.; Gilson, M. K.; Briggs, J. M.; Humblet, C.; Sussman, J. L. Binding of Tacrine and 6-Chlorotacrine by Acetylcholinesterase. *Biopolymers* **1996**, *38*, 109–117.
(87) Recanatini, M.; Cavalli, A.; Belluti, F.; Piazzi, L.; Rampa, A.; Bisi, A.; Gobbi, S.; Valenti, P.; Andrisano, V.; Bartolini, M.; Cavrini, V. SAR of 9-Amino-1,2,3,4-tetrahydroacridine-Based Acetylcholinesterase Inhibitors: Synthesis, Enzyme Inhibitory Activity, QSAR, and Structure-Based CoMFA of Tacrine Analogues. *J. Med. Chem.* **2000**, *43*, 2007–2018.
(88) Bartolini, M.; Bertucci, C.; Cavrini, V.; Andrisano, V. *β*-Amyloid Aggregation Induced by Human Acetylcholinesterase: Inhibition Studies. *Biochem. Pharmacol.* **2003**, *65*, 407–416.
(89) Jakob-Roetne, R.; Jacobsen, H. Alzheimer's Disease: From Pathology to Therapeutic Approaches. *Angew. Chem., Int. Ed.* **2009**, *48*, 3030–3059.
(90) Mancini, F.; Naldi, M.; Cavrini, V.; Andrisano, V. Multiwell Fluorometric and Colorimetric Microassays for the Evaluation of Beta-Secretase (BACE-1) Inhibitors. *Anal. Bioanal. Chem.* **2007**, *388*, 1175–1183.
(91) Fu, H.; Li, W.; Luo, J.; Lee, N. T. K.; Li, M.; Tsim, K. W. K.; Pang, Y.; Youdim, M. B. H.; Han, Y. Promising Anti-Alzheimer's Dimer Bis(7)-tacrine Reduces *β*-Amyloid Generation by Directly Inhibiting BACE-1 Activity. *Biochem. Biophys. Res. Commun.* **2008**, *366*, 631–636.
(92) Rosini, M.; Andrisano, V.; Bartolini, M.; Melchiorre, C. Organic Compounds Useful for the Treatment of Alzheimer's Disease, Their Use and Method of Preparation. WO 2006/080043 A2, 2006.
(93) Piazzi, L.; Cavalli, A.; Colizzi, F.; Belluti, F.; Bartolini, M.; Mancini, F.; Recanatini, M.; Andrisano, V.; Rampa, A. Multi-Target-Directed Coumarin Derivatives: hAChE and BACE1 Inhibitors as Potential Anti-Alzheimer Compounds. *Bioorg. Med. Chem.* **2008**, *18*, 423–426.
(94) Hanessian, S.; Yun, H.; Hou, Y.; Yang, G.; Bayrakdarian, M.; Therrien, E.; Moitessier, N.; Roggo, S.; Veenstra, S.; Tintelnot-Blomley, M.; Rondeau, J.-M.; Ostermeier, C.; Strauss, A.; Ramage, P.; Paganetti, P.; Neumann, U.; Betschart, C. Structure-Based Design, Synthesis, and Memapsin 2 (BACE) Inhibitory Activity of Carbocyclic and Heterocyclic Peptidomimetics. *J. Med. Chem.* **2005**, *48*, 5175–5190.
(95) Di, L.; Kerns, E. H.; Fan, K.; McConnell, O. J.; Carter, G. T. High Throughput Artificial Membrane Permeability Assay for Blood−Brain Barrier. *Eur. J. Med. Chem.* **2003**, *38*, 223–232.
(96) Reviriego, F.; Rodríguez-Franco, M. I.; Navarro, P.; García-España, E.; Liu-González, M.; Verdejo, B.; Domènech, A. The Sodium Salt of Diethyl 1*H*-Pyrazole-3,5-dicarboxylate as an Efficient Amphiphilic Receptor for Dopamine and Amphetamines. Crystal Structure and Solution Studies. *J. Am. Chem. Soc.* **2006**, *128*, 16458–16459.
(97) Pavón, F. J.; Hernández-Folgado, L.; Bilbao, A.; Cippitelli, A.; Jagerovic, N.; Abellán, G.; Rodríguez-Franco, M. I.; Serrano, A.; Macías, M.; Navarro, M.; Goya, P.; Rodríguez de Fonseca, F. Antiobesity Effects of the Novel in Vivo Neutral Cannabinoid Receptor Antagonist 5-(4-Chlorophenyl)-1-(2,4-dichlorophenyl)-3-hexyl-1*H*-1,2,4-triazole—LH 21. *Neuropharmacology* **2006**, *51*, 358–366.
(98) Marco-Contelles, J.; León, R.; de los Ríos, C.; Samadi, A.; Bartolini, M.; Andrisano, V.; Huertas, O.; Barril, X.; Luque, F. J.; Rodríguez-Franco, M. I.; López, B.; López, M. G.; García, A. G.; Carreiras, M. C.; Villarroya, M. Tacripyrines, the First Tacrine−Dihydropyridine Hybrids, as Multitarget-Directed Ligands for the Treatment of Alzheimer's Disease. *J. Med. Chem.* **2009**, *52*, 2724–2732.
(99) Bartolini, M.; Bertucci, C.; Bolognesi, M. L.; Cavalli, A.; Melchiorre, C.; Andrisano, V. Insight into the Kinetic of Amyloid Beta (1−42) Peptide Self-Aggregation: Elucidation of Inhibitors' Mechanism of Action. *ChemBioChem* **2007**, *8*, 2152–2161.
(100) Morley, S. D.; Afshar, M. Validation of an Empirical RNA-Ligand Scoring Function for Fast Flexible Docking Using Ribo-Dock. *J. Comput.-Aided Mol. Des.* **2004**, *18*, 189–208.
(101) Barril, X.; Hubbard, R. E.; Morley, S. D. Virtual Screening in Structure-Based Drug Discovery. *Mini-Rev. Med. Chem.* **2004**, *4*, 779–791.
(102) *ACD/pKa*, version 8.02; Advanced Chemistry Development, Inc.: Toronto, Ontario, Canada, 2006; www.acdlabs.com.
(103) Dewar, M. J. S.; Zoebisch, E. G.; Healy, E. F.; Stewart, J. J. P. AM1: A New General Purpose Quantum Mechanical Molecular Model. *J. Am. Chem. Soc.* **1985**, *107*, 3902–3909.
(104) Frisch, M. J.; Trucks, G. W.; Schlegel, H. B.; Scuseria, G. E.; Robb, M. A.; Cheeseman, J. R.; Montgomery, J. A., Jr.; Vreven, T.; Kudin, K. N.; Burant, J. C.; Millam, J. M.; Iyengar, S. S.; Tomasi, J.; Barone, V.; Mennucci, B.; Cossi, M.; Scalmani, G.; Rega, N.; Petersson, G. A.; Nakatsuji, H.; Hada, M.; Ehara, M.; Toyota, K.; Fukuda, R.; Hasegawa, J.; Ishida, M.; Nakajima, T.; Honda, Y.; Kitao, O.; Nakai, H.; Klene, M.; Li, X.; Knox, J. E.; Hratchian, H. P.; Cross, J. B.; Adamo, C.; Jaramillo, J.; Gomperts, R.; Stratmann, R. E.; Yazyev, O.; Austin, A. J.; Cammi, R.; Pomelli, C.; Ochterski, J. W.; Ayala, P. Y.; Morokuma, K.; Voth, G. A.; Salvador, P.; Dannenberg, J. J.; Zakrzewski, V. G.; Dapprich, S.; Daniels, A. D.; Strain, M. C.; Farkas, O.; Malick, D. K.; Rabuck, A. D.; Raghavachari, K.; Foresman, J. B.; Ortiz, J. V.; Cui, Q.; Baboul, A. G.; Clifford, S.; Cioslowski, J.; Stefanov, B. B.; Liu, G.; Liashenko, A.; Piskorz, P.; Komaromi, I.; Martin, R. L.; Fox, D. J.; Keith, T.; Al-Laham, M. A.; Peng, C. Y.; Nanayakkara, A.; Challacombe, M.; Gill, P. M. W.; Johnson, B.; Chen, W.; Wong, M. W.; Gonzalez, C.; Pople, J. A. *Gaussian 03*, revision B.04, Gaussian, Inc.: Pittsburgh PA, 2003.
(105) Case, D. A.; Darden, T. A.; Cheatham, T. E., III; Simmerling, C. L.; Wang, J.; Duke, R. E.; Luo, R.; Merz, K. M.; Pearlman, D. A.; Crowley, M.; Walker, R. C.; Zhang, W.; Wang, B.; Hayik, S.; Roitberg, A.; Seabra, G.; Wong, K. F.; Paesani, F.; Wu, X.; Brozell, S.; Tsui, V.; Gohlke, H.; Yang, L.; Tan, C.; Mongan, J.; Hornak, V.; Cui, G.; Beroza, P.; Mathews, D. H.; Schafmeister, C.; Ross, W. S.; Kollman, P. A. *AMBER*, version 9; University of California: San Francisco, CA, 2006.
(106) Bayly, C. I.; Cieplak, P.; Cornell, W. D.; Kollman, P. A. A Well-Behaved Electrostatic Potential Based Method Using Charge Restraints for Deriving Atomic Charges. *J. Phys. Chem.* **1993**, *97*, 10269–10280.
(107) Sitkoff, D.; Sharp, K. A.; Honig, B. Accurate Calculation of Hydration Free Energies Using Macroscopic Solvent Models. *J. Phys. Chem.* **1994**, *98*, 1978–1988.
(108) Eldridge, M. D.; Murray, C. W.; Auton, T. R.; Paolini, G. V.; Mee, R. P. Empirical Scoring Functions: I. The Development of a Fast Empirical Scoring Function To Estimate the Binding Affinity of Ligands in Receptor Complexes. *J. Comput.-Aided Mol. Des.* **1997**, *11*, 425–445.
(109) Camps, P.; Gómez, E.; Muñoz-Torrero, D.; Badia, A.; Clos, M. V.; Curutchet, C.; Muñoz-Muriedas, J.; Luque, F. J. Binding of 13-Amidohuprines to Acetylcholinesterase: Exploring the Ligand-Induced Conformational Change of the Gly117−Gly118 Peptide Bond in the Oxyanion Hole. *J. Med. Chem.* **2006**, *49*, 6833–6840.
(110) Barril, X.; Orozco, M.; Luque, F. J. Predicting Relative Binding Free Energies of Tacrine−Huperzine A Hybrids as Inhibitors of Acetylcholinesterase. *J. Med. Chem.* **1999**, *42*, 5110–5119.
(111) Jorgensen, W. L.; Chandrasekhar, J.; Madura, J. D.; Impey, R. W.; Klein, M. L. Comparison of Simple Potential Functions for Simulating Liquid Water. *J. Chem. Phys.* **1983**, *79*, 926–935.